NAVAL POSTGRADUATE SCHOOL

MONTEREY, CALIFORNIA

THESIS

IMPROVED ATOM COUNTING USING SQUEEZED LIGHT FOR ATOM INTERFEROMETRY APPLICATIONS

by

Mark D. Vetere

June 2022

Thesis Advisor: Frank A. Narducci
Second Reader: Jeffrey G. Lee

THIS PAGE INTENTIONALLY LEFT BLANK

REPORT DOCUMENTATION PAGE			*Form Approved OMB No. 0704-0188*

1. AGENCY USE ONLY *(Leave blank)*	**2. REPORT DATE** June 2022	**3. REPORT TYPE AND DATES COVERED** Master's thesis

4. TITLE AND SUBTITLE
IMPROVED ATOM COUNTING USING SQUEEZED LIGHT FOR ATOM INTERFEROMETRY APPLICATIONS

5. FUNDING NUMBERS

6. AUTHOR(S) Mark D. Vetere

7. PERFORMING ORGANIZATION NAME(S) AND ADDRESS(ES)
Naval Postgraduate School
Monterey, CA 93943-5000

8. PERFORMING ORGANIZATION REPORT NUMBER

9. SPONSORING / MONITORING AGENCY NAME(S) AND ADDRESS(ES)
N/A

10. SPONSORING / MONITORING AGENCY REPORT NUMBER

11. SUPPLEMENTARY NOTES The views expressed in this thesis are those of the author and do not reflect the official policy or position of the Department of Defense or the U.S. Government.

12a. DISTRIBUTION / AVAILABILITY STATEMENT
Approved for public release. Distribution is unlimited.

12b. DISTRIBUTION CODE
A

13. ABSTRACT (maximum 200 words)

Atom interferometer measurements are affected by the amount of quantum noise from the laser used to detect atoms. To improve the quantum limited sensitivity of interferometers, there needs to be a way to reduce the amount of quantum noise. Light is composed of two quadratures, where the product of the noise in each quadrature cannot be below a minimum threshold set by the Heisenberg Uncertainty Principle. However, the noise in one quadrature can be reduced at the expense of the other. This form of light is referred to as "squeezed light." Squeezed light can be produced using four-wave mixing (FWM). Electromagnetically induced transparency (EIT) is an interference phenomenon that occurs when a three-level atom is driven by a coherent field that makes a non-linear medium transparent to the probing field and holds a great deal of similarities to FWM. This thesis developed a theoretical framework that describes the measurement of atomic states and associated noise when quantum light is used to drive the atom and lays the groundwork to produce squeezed light through developing an experiment to produce EIT, as well as discussing the similarities between EIT and FWM to create and further study FWM for improved atom interferometry.

14. SUBJECT TERMS	**15. NUMBER OF PAGES**
squeezed light, atom interferometer, four-wave mixing, FWM, inertial navigation, gyroscope, accelerometers, electromagnetically induced transparency, EIT	77
	16. PRICE CODE

17. SECURITY CLASSIFICATION OF REPORT	**18. SECURITY CLASSIFICATION OF THIS PAGE**	**19. SECURITY CLASSIFICATION OF ABSTRACT**	**20. LIMITATION OF ABSTRACT**
Unclassified	Unclassified	Unclassified	UU

NSN 7540-01-280-5500

Standard Form 298 (Rev. 2-89)
Prescribed by ANSI Std. 239-18

THIS PAGE INTENTIONALLY LEFT BLANK

Approved for public release. Distribution is unlimited.

IMPROVED ATOM COUNTING USING SQUEEZED LIGHT FOR ATOM INTERFEROMETRY APPLICATIONS

Mark D. Vetere
Captain, United States Marine Corps
BS, United States Naval Academy, 2015

Submitted in partial fulfillment of the
requirements for the degree of

MASTER OF SCIENCE IN APPLIED PHYSICS

from the

NAVAL POSTGRADUATE SCHOOL
June 2022

Approved by: Frank A. Narducci
Advisor

Jeffrey G. Lee
Second Reader

Joseph P. Hooper
Chair, Department of Physics

THIS PAGE INTENTIONALLY LEFT BLANK

ABSTRACT

Atom interferometer measurements are affected by the amount of quantum noise from the laser used to detect atoms. To improve the quantum limited sensitivity of interferometers, there needs to be a way to reduce the amount of quantum noise. Light is composed of two quadratures, where the product of the noise in each quadrature cannot be below a minimum threshold set by the Heisenberg Uncertainty Principle. However, the noise in one quadrature can be reduced at the expense of the other. This form of light is referred to as "squeezed light." Squeezed light can be produced using four-wave mixing (FWM). Electromagnetically induced transparency (EIT) is an interference phenomenon that occurs when a three-level atom is driven by a coherent field that makes a non-linear medium transparent to the probing field and holds a great deal of similarities to FWM. This thesis developed a theoretical framework that describes the measurement of atomic states and associated noise when quantum light is used to drive the atom and lays the groundwork to produce squeezed light through developing an experiment to produce EIT, as well as discussing the similarities between EIT and FWM to create and further study FWM for improved atom interferometry.

THIS PAGE INTENTIONALLY LEFT BLANK

Table of Contents

THIS PAGE INTENTIONALLY LEFT BLANK

List of Figures

THIS PAGE INTENTIONALLY LEFT BLANK

List of Acronyms and Abbreviations

DFB	distributed feedback laser
EIT	electromagnetically induced transparency
EMCON	Emission Control
FWHM	full width at half maximum
FWM	four-wave mixing
GPS	Global Positioning System
HFAOM	high frequency acousto-optic modulator
INS	inertial navigation systems
LFAOM	low frequency acousto-optic modulator
MEMS	micro-electrical-mechanical systems
NPS	Naval Postgraduate School
RLGs	ring laser gyroscopes
SQL	standard quantum limit

THIS PAGE INTENTIONALLY LEFT BLANK

Acknowledgments

To my advisor, Dr. Frank Narducci, thank you for the astronomical number of hours spent working with me. As difficult and sometimes frustrating as it was to work on this thesis, I am extremely happy in my choice to work with you and on this project. I have learned more than I ever thought possible and it is because of you. I am forever grateful for your willingness to help, coach, mentor, and teach me to accomplish this goal, even if I was not the easiest to help, coach, mentor, or teach. Sincerely, thank you.

To Dr. Jeff Lee, thank you for answering all of my questions, even the same ones I asked you the day prior. I had zero knowledge of how the lab, lasers, or equipment worked upon starting this thesis and you very willingly took the time to guide me to be successful. Thank you for teaching me how to assemble the hardware, explaining what each part does, building electronics for the experiment, and constantly reminding me how to fix the settings I changed incorrectly on the oscilloscope.

Finally, thank you to my parents, for always supporting me and making sure I stayed focused and completed my goal no matter what got in the way.

To anyone who reads this too, thank you.

Now, for some light reading.

THIS PAGE INTENTIONALLY LEFT BLANK

CHAPTER 1:
Introduction

Currently, throughout the armed forces there is an admittedly heavy reliance on the Global Positioning System (GPS) for finding one's location on the earth and for navigation. A wide range of systems depend on GPS, from GPS-guided munitions to surface ships and aircraft. However, there are many scenarios in which the GPS signal can be spoofed, compromised, or be completely blocked. These scenarios range from operations in GPS-jammed environments to operations under the water where GPS signals cannot propagate to aircraft operating under Emission Control (EMCON). In the absence of GPS, platforms need to depend on their on-board inertial navigation systems (INS). These are systems comprised of accelerometers and gyroscopes that measure linear acceleration and angular velocity and compute a platform's current location based on these measurements and the known prior location.

In inertial systems, the output from the gyroscope (assuming the gyroscope is a *rate* gyroscope-meaning it measures a rotation rate) is integrated up to find the new angular heading (yaw, pitch and roll). These updated headings, along with the reading from the accelerometers, are entered into the equations of motion for a rigid rotating body. These equations are integrated up twice to obtain position. Because the position readouts are integrated up twice and the rotation rate readouts are effectively integrated three times, the final navigation solution is sensitive to many sources of error, ranging from numerical noise in the integrator to error in the actual measurements. Of particular relevance to this thesis are the measurement errors and in particular, two kinds: random walk errors and bias drift. This discussion focuses on gyroscope measurement errors because that system usually produces the larger error, due to the three integrations of the output. However, accelerometers have very similar errors. The first type of error is commonly referred to as *angle random walk*. Noise in the rate measurement will result in noise in the angle heading and can be thought of as "jitter" in the heading measurement. *Bias drift* is the second type of noise. A gyroscope will often read a non-zero value for the rotational rate, even for a platform that is perfectly stationary. This non-zero reading is known as the *bias* and could be subtracted out before integration except for the fact that it is usually not constant in time. Both errors integrate up and result in a discrepancy between the location "truth" and the

sensor location. Gyroscopes also suffer from *scale factor instability*. In a gyroscope, what is measured is a voltage arising from an electrical signal from the measurement. The voltage is converted to the quantity of interest-the rotation rate-through a series of scale factors. These scale factors are often also not constant in time: they can depend on environmental conditions (e.g., temperature, barometric pressure, humidity). All of these errors result in a position error that accumulates cubically with the time since the last GPS fix (quadratically, in the case of accelerometers).

Systems where accuracy is required only over very short time spans commonly use micro-electrical-mechanical systems (MEMS) gyroscopes. These systems include cell phones, where the position of the phone is nearly always updated by GPS, or GPS-guided munitions in which the flight time is short. For applications requiring accuracy for longer periods of time (e.g., longer flights or submarine applications), very expensive and highly stabilized gyroscopes based on ring laser gyroscopes (RLGs) are used. However, even the very high-end systems are prone to the measurement errors previously described. As a result, it is highly desirable to develop systems with smaller errors. The emerging technology based on quantum sensors and specifically atom interferometer sensors offer a very promising advancement to inertial navigation. Atom-based gyroscopes offer a potential improvement over otherwise equal light-based gyroscope systems of up to 11 *orders of magnitude* [1]. This extreme factor stems from the mass scaling: an atom's mass is 11 orders of magnitude larger than the effective photon mass, m_{photon}, derived from setting the photon energy as defined by Planck $E = \hbar\omega$, where $\hbar$ is the reduced Planck's constant and ω is the angular frequency of the photon, to the Einstein energy $E = m_{photon}c^2$. However, this number does not represent the real improvement of atom-based sensors over light-based sensors. Atom sources are not as "bright" as the laser sources used in RLGs and photons can be stored in ring resonators and make thousands of passes, while atoms (currently) can only pass through an interferometer once. However, taking these effects into account, three to four orders of magnitude improvement is achievable. Various types of atom interferometers have been demonstrated [2]–[5] and the initial performance numbers (e.g., [6]–[9]) are quite impressive, and a number of review articles have been written [10]–[17].

The work being reported on in this thesis is motivated by trying to improve on the already impressive sensitivity of atom interferometers by reducing the noise in the "read-out" stage of the interferometer. A typical atom interferometer consists of a beam of atoms or a "pulse" of atoms traveling along a trajectory. The atoms are subjected to a series of optical pulses

that are specially tailored so that the atoms' path is split, redirected and recombined in very much the same manner as in an optical interferometer (e.g., a Mach-Zehnder interferometer). The path information is stored in the phase accumulated by the atoms in each trajectory and then the two phases are subtracted with the final recombining pulse. The phase difference is read out by detecting which state the atom is in, since the probability of finding the atom in one state versus the other varies with the phase difference.

The states to be detected are usually two ground states because there is no spontaneous emission between the two states and very little incoherent transfer of population from other physical mechanisms such as collisions. For the sake of this discussion, we will label the states using the Dirac notion $|1\rangle$ and $|2\rangle$. The atom also has an excited state that is usually accessible from either ground state by optically driving the transition with a laser. The transition frequencies of the two transitions $|1\rangle \rightarrow |3\rangle$ and $|2\rangle \rightarrow |3\rangle$ are sufficiently different from each other that the two transitions can be spectroscopically distinguished. By turning on a laser at the right frequency, the atom will fluoresce and the amount of fluorescence is proportional to the number of atoms in that state. It is this stage of the readout that the work in this thesis is addressing. As described, the fluorescence is caused by a laser, which is inherently a noisy device. The lasers used in the Naval Postgraduate School (NPS) Quantum Sensors Lab are semi-conductor lasers. Fluctuations in the current supply, the temperature controller, and a myriad of other effects in the lab can lead to frequency fluctuations of the laser. However, these can be considered as *technical noise* and can, at least in principle, be eliminated. However, all electromagnetic fields, including fields from the laser, have inherent *quantum* noise that cannot be eliminated. This noise is present on the laser that is used to measure the atomic states, leading to noise in the measurement, lower signal-to-noise and hence, decreased sensitivity. There are certain kinds of laser fields, however, in which the noise in one channel can be reduced below the quantum limit at the expense of increased noise in another channel. These states of light are known as *squeezed light*.

The work of this thesis is motivated by trying to use the reduced-noise channel of a squeezed field as the detection field in an atom interferometer for the purpose of improved signal-to-noise. In the background chapter, Chapter 2, we review the theory of the interaction of light with atoms: a building block for all the physics phenomena discussed in the rest of the thesis. Building on that section, we then discuss the two basic processes that are used in atom interferometry, namely, the Raman and Ramsey processes.

In Chapter 3, we present fully quantum calculations that describe the interaction of an atom in an atomic beam with quantum fields of light. From these calculations, we extract the probability of finding the atom in the excited state, which is what is measured in the experiment, along with an expression for the noise associated with that measurement. We apply the developed framework to two types of quantum states: a coherent state, and a two-photon squeezed state. Although much more analysis needs to be performed, we demonstrate that the framework can be used to study the use of quantum states of light in interferometry.

We discuss some preliminary experiments in Chapter 4. Having argued that the use of squeezed light fields is beneficial to atom interferometry, it would be useful to know how to generate such fields in a manner useful for the integration with the existing atom interferometers in the NPS Quantum Sensors Lab, which utilize rubidium (specifically the ^{85}Rb isotope). The generation of squeezed light can be achieved through a process of four-wave mixing (FWM) in a gas of atoms. A main requirement for this process to work is the development of coherence between the two ground states. An excellent way to measure the ground state coherence is through a process known as electromagnetically induced transparency (EIT). We discuss this process and the experiment we performed to measure the ground state coherence, after demonstrating that the setup should work for FWM. Although time constraints prevented the demonstration of the FWM, the experiment is outlined.

Finally, Chapter 5 addresses outlook and future work.

CHAPTER 2:
Background

As discussed in detail in Chapter 1, the main purpose of this thesis is to describe the mating of quantum squeezed light with an atom interferometer, with the goal of improving the signal-to-noise ratio in the measurement of phase from the interferometer, which ultimately leads to improved sensitivity of atom-based sensors (e.g., gyroscopes and accelerometers). The basic building blocks of an atom interferometer as well as the process for making squeezed light depends on the interaction of light with atomic systems. This chapter discusses some of the basic processes that are relevant to this work. We begin by considering the interaction of a single-mode laser field with a simple two-level atom, followed by a discussion of Raman and Ramsey spectroscopy. We next turn to a discussion of the so-called *electromagnetically induced transparency* (EIT) phenomenon, which we used as a diagnostic for our system. Finally, we discuss *four-wave mixing* (FWM) and the generation of squeezed light. The material in this chapter lays the groundwork for the calculations presented in Chapter 4.

2.1 The Two-Level Atom

We begin this section by discussing the interaction of a single-mode laser and a two-level atom. This problem is one routinely discussed in many books on quantum optics [18]–[20]. In this section, we simply present the highlights.

Atoms consist of many electronic energy levels, sometimes referred to as orbitals. Standard quantum mechanics classes show students how to calculate the energy levels in hydrogen (see e.g., [21], [22]). Energy levels in more complicated atoms are, by their very nature, more complicated, but the basic physics is the same. "Real" atoms have a large number of electronic orbitals; often, however, it is useful to make the approximation that all the energy levels are sufficiently far apart energetically such that there are only a few energy levels of interest (in this case, two). These energy levels can be denoted using Dirac *bra-ket* notation by $|1\rangle$ and $|2\rangle$, where $|1\rangle$ represents the orbital (energy level) with lower energy, and $|2\rangle$ represents the orbital (energy level) with higher energy. These energy levels are depicted in Figure 2.1. As taught to us by Louis deBroglie [23], the energy difference ΔE between the two energy states is related to the atomic transition frequency ω_A by $\Delta E = \hbar\omega_A$, where $\hbar$

is the reduced Planck's constant. The two levels also form a dipole moment that we denote $\boldsymbol{\mu}_{12}$.

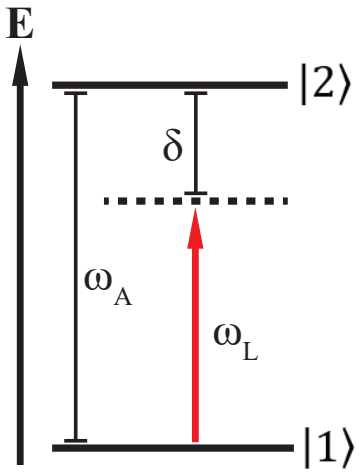

Figure 2.1. Single-mode field interacting with a two-level atom.

Also depicted in the figure is a single-mode laser field of frequency ω_L, field amplitude $\mathcal{E}$ and polarization vector $\boldsymbol{\varepsilon}_L$. The light interacts with the atoms and can change the probability of finding the atom in state $|1\rangle$ or state $|2\rangle$ dynamically. In particular, if the atom is initially prepared in state $|1\rangle$ at time $t = 0$, then the probability of finding the atom in the excited state $|2\rangle$, $P_2(t)$ after some time t is given by

$$P_{|2\rangle}(t) = \frac{1}{2}\left|\frac{\Omega}{\Omega'}\right|^2 (1 - \cos\Omega' t)\,. \tag{2.1a}$$

In Equation 2.1a, Ω is the so-called *Rabi frequency*, given by

$$\Omega = \frac{2(\boldsymbol{\mu}_{12}^* \cdot \boldsymbol{\varepsilon}_L \mathcal{E})}{\hbar}, \tag{2.1b}$$

Ω' is the *generalized Rabi frequency*

$$\Omega' = \sqrt{|\Omega|^2 + \delta^2}, \tag{2.1c}$$

and δ is the mismatch between the laser frequency and the atomic transition frequency,

known more commonly as the *detuning*

$$\delta = \omega_L - \omega_A. \tag{2.1d}$$

A plot of Equation 2.1a as a function of time for three different values of the detuning can be found in Figure 2.2. This continuous change of probability of finding atoms in the excited

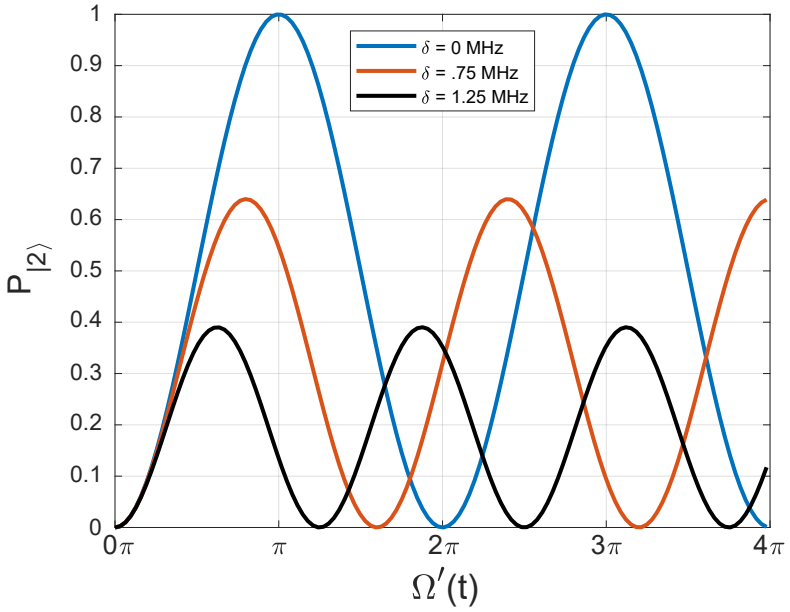

Figure 2.2. Rabi oscillations for varying values of detuning. $\Omega = 1.0$MHz.

state in a sinusoidal manner is called Rabi oscillation or Rabi flopping [18]. From Equation 2.1c and Figure 2.2 we see that the generalized Rabi frequency depends on the detuning: as the detuning increases the Rabi frequency increases. However, there is a downfall when the detuning is non-zero. From the same equation we can see that Ω' will always be greater than Ω. Hence, from Equation 2.1a, $P_2(t)$ will never equal 1, implying that the atoms can never fully be in the excited state. We can think of the Ω/Ω' as an efficiency term with respect to detuning.

As the atoms undergo Rabi oscillations between state $|1\rangle$ and $|2\rangle$, one important process occurs when the atom returns to the ground state. Conservation of energy tells us that in order to transition to a higher energy state, energy must be added to the system. The opposite is also true when returning from the excited state to the ground state, except that

energy must be released from the system. In the case of Rabi oscillations, the energy is released in the form of a photon. This is called *stimulated emission*. When the atom emits a photon due to stimulated emission the photon is emitted in phase with the driving field of the laser. This is important because there is nothing that interrupts the Rabi cycle and so it continues as normal.

There is a second process called *spontaneous emission* that also occurs when an atom transitions from an unstable excited state to a ground state. The spontaneously emitted photon is emitted in a random direction with a random phase with respect to the driving field and the Rabi cycle starts all over again. For this experiment, it is safe to make the assumption that spontaneous emission can be ignored: spontaneous emission only occurs between an excited state and a ground state. In this experiment, when we apply the Raman or Ramsey pulses, the combination of the two fields act as a single laser and they drive the ground state transition, where there is no spontaneous emission. This will be explored in greater detail in Section 2.2.

By changing the duration of the field probing the transition we can determine the probability of finding atoms in the excited state based on Equation 2.1a. Assuming a resonant probing field, Figure 2.2 depicts two Rabi cycles, where the cycle time is the time it takes for the atom to transition from the ground state to the excited state and then return to the ground state. When the probing field is on-resonance, a complete cycle occurs every $t = 2\pi/\Omega$. Thus, if we turn the probing laser on for $t = 2\pi/\Omega$ and then measure the state of the atoms, we will find that the atoms have returned to the ground state. If we shorten the time that the probing field is on, again assuming on-resonance, to $t = \pi/\Omega$, then we know the probability of finding the atoms in the excited state is equal to 1, again according to Equation 2.1a. This type of a pulse is called a π-pulse. If we further shorten the time the resonant probing field is on to $t = \pi/2\Omega$ then we find that $P_2(t) = .5$. This value for the probability means that the atoms are in a coherent superposition between state $|1\rangle$ and $|2\rangle$ [24].

These values for t in the cases of π-pulses and $\pi/2$-pulses are only true when the probing field is on-resonance. As the probing field is detuned, the relative time of a detuned π-pulse or $\pi/2$-pulse is less than a resonant π-pulse since the Rabi frequency increases as detuning increases. However, the basic cycle stays the same, one cycle is 2π, similar to a standard sine or cosine wave. However, as pointed out earlier, the atom never becomes fully excited.

When an atomic state is measured, the atoms can only be found in the ground state or

the excited state–there is no middle ground. In this sense, the plot in Figure 2.2 can be misleading. Since the plot is really a depiction of probability, as we shorten the time of the pulses we are decreasing the probability that the atom will be excited. Having a lower probability of exciting the atom is not ideal for an interferometer, which we will discuss later in the paper.

2.2 Three-Level Atom

We now turn to a discussion of the interaction of two single-mode lasers with a three-level atom. A three-level atom is constructed of two lower levels, $|1\rangle$ and $|2\rangle$, and a third higher energy level, $|3\rangle$ as depicted in Figure 2.3. Each lower level is coupled to $|3\rangle$, with level $|3\rangle$ representing the excited state [18]. In the atoms in our experiments, the transition frequencies ω_{13} and ω_{23} are in the optical part of the spectrum, while the ground state separation (energy between states $|1\rangle$ and $|2\rangle$) is in the microwave portion of the spectrum.

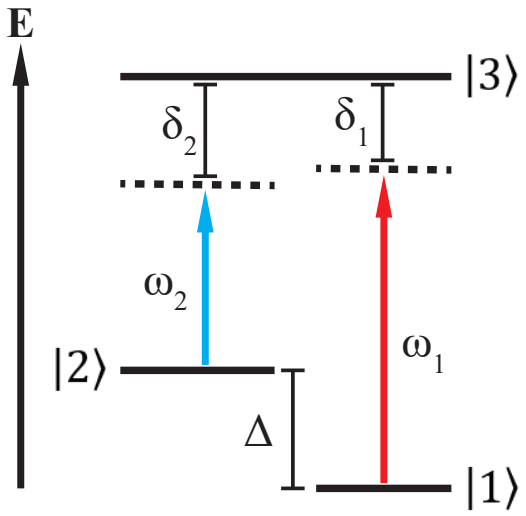

Figure 2.3. Energy level diagram of a three-level atom.

In this case, we have two different single-mode driving laser fields of frequencies ω_1 and ω_2. Just as in the case of the two-level atom in the previous section, the frequencies of these driving fields need not be on-resonance; in fact, in our experiments, they are *far* from resonance. The mismatches between laser frequencies and their respective transitions,

depicted in Figure 2.3 by δ_1 and δ_2, are defined by the *single-photon detuning* terms, as

$$\delta_1 = \omega_1 - \omega_{13} \tag{2.2a}$$

$$\delta_2 = \omega_2 - \omega_{23}. \tag{2.2b}$$

Two-photon detuning, δ_{2p} is defined as the mismatch between the frequency difference between the two laser fields with respect to the hyperfine transition frequency, Δ. Two-photon detuning is given by

$$\begin{aligned} \delta_{2p} &= \omega_1 - \omega_2 - \Delta \\ &= \omega_1 - \omega_2 - (\omega_{13} - \omega_{23}) \\ &= (\omega_1 - \omega_{13}) - (\omega_2 - \omega_{23}) \\ &= \delta_1 - \delta_2, \end{aligned} \tag{2.3}$$

where ω_{13} and ω_{23} are the atomic transition frequencies between states $|1\rangle$ and $|3\rangle$ and states $|2\rangle$ and $|3\rangle$, respectively.

In the case of the atom interferometer, spontaneous emission must be avoided at all costs because spontaneous emission destroys the coherence required to see interference. Therefore, driving a single photon electronic transition in general does not work, although there are some very narrow transitions [25], such as strontium, that can be used for interferometers. It is for this reason that Raman transitions are often used. Raman transitions are transitions between the two ground states.

To drive Raman transitions, δ_1 and δ_2 must be large relative to the atomic transition decay rates, making the laser fields far off-resonance from their respective transition frequencies. Since they are so far off-resonance there is little to no interaction between the lower levels and state $|3\rangle$. Because there is no interaction with $|3\rangle$ there is very little population in state $|3\rangle$, and therefore it can be adiabatically eliminated from the equations, and what is left are equations for $|1\rangle$ and $|2\rangle$. These equations are analogous to the two-level atom equations previously described, where we have Rabi cycling and all the same physics as the driven two-level atom problem. However, because the relevant states are the two ground states,

there is no spontaneous emission.

It should be stressed that to drive Raman transitions in a three-level atom, there must be two driving fields, labeled as ω_1 and ω_2. These two lasers act as one driving field driving the ground state transition. We often call this arrangement of two laser frequencies close to two-photon resonance the *Raman field*, and it plays the role of the single laser in the two-level atom problem. In deriving the three-level atom equations with state $|3\rangle$ adiabatically eliminated, a detuning term analogous to the two-level atom system is found,

$$\delta_{2p} = \delta_1 - \delta_2 - \delta_{AC}, \tag{2.4a}$$

where δ_{AC} is referred to as the differential AC Stark shift and is equal to

$$\delta_{AC} = \left(\frac{|\Omega_1|^2}{\delta_1} - \frac{|\Omega_2|^2}{\delta_2} \right). \tag{2.4b}$$

For Raman transitions, δ_1 and δ_2 are large and as a result by definition in Equation 2.4b δ_{AC} will be small. Additionally, we can also choose our Rabi frequencies, Ω_1 and Ω_2, to be very close or exactly the same, and when $\delta_1 = \delta_2$, $\delta_{AC} = 0$. So, for the rest of this discussion, we will assume $\delta_{AC} = 0$. In this situation, δ_{2p} as defined by Equations 2.3 and 2.4a are identical.

Having considered the Raman laser field and two-photon detuning, we can now discuss the probability of finding the atom excited after being illuminated by the Raman field. In this case, the term "excited" refers to finding the atom in the upper ground state, ($|2\rangle$). Once again, in analogy to the two-level atom problem, the atoms are initially prepared in state $|1\rangle$ at time $t = 0$, then the probability of finding the atom in the excited state after some time t is given by

$$P_{|2\rangle}(t) = \frac{1}{2} \left| \frac{\Omega_R}{\Omega'_R} \right|^2 \left(1 - \cos \Omega'_R t \right), \tag{2.4c}$$

where Ω_R is the Raman Rabi frequency, which equals

$$\Omega_R = \frac{\Omega_1^* \Omega_2}{2\delta} \tag{2.4d}$$

with Ω_1 and Ω_2 being the single-photon Rabi frequency, the same as Equation 2.1b relative

to the respective transitions. Here, δ has no subscript because one can take it to be *either* δ_1 or δ_2. Since we assume both δ_1 and δ_2 are large and differ from one another by a very small amount since we operate close to two-photon resonance, the simplification is made in Equation 2.4d to simply write δ. Just like in the two-level atom we have a generalized Raman Rabi frequency given by

$$\Omega_R' = \sqrt{|\Omega_R|^2 + \delta_{2p}^2}. \tag{2.4e}$$

The main takeaway from this section is that the physics of an atom interferometer using three-level atoms acts the same as the physics governing a two-level atom. We will discuss more regarding how atom interferometers work in our discussion about Raman and Ramsey spectroscopy.

2.3 Raman Spectroscopy

In this section, we discuss Raman spectroscopy. This technique is useful for finding the precise frequency of an atomic transition. In the case of the atoms being used in the NPS Quantum Sensors lab, the frequency corresponds to the ground state energy difference as discussed in the previous section. It is also the main process used in the construction of an atom interferometer.

We begin by showing how to use Equation 2.4c to find the frequency of the transition between states $|1\rangle$ and $|2\rangle$. Initially, we are going to assume that we are on two-photon resonance, which means δ_{2p} in Equation 2.4a equals zero. We can simplify Equation 2.4c to be

$$P_{|2\rangle}(t) = \frac{1}{2}\left(1 - \cos\Omega_R t\right). \tag{2.5}$$

With a two-level atom, we know that when our exciting laser field, ω_L is far off resonance, we will see very little excitation of the atoms. As we change the frequency of ω_L closer to resonance we see increased excitation of the atoms. When we reach a maximum, we know that we have found our transition frequency, and $\omega_L = \omega_A$. There is an analogous process in the three-level atom problem. We can tune both lasers far from single-photon resonance and initially also far from two-photon resonance. If all the atoms start in the lower ground state, there will be very little excitation to the upper ground state (the excited state). As the

two-photon detuning is decreased, the excitation increases until it reaches a maximum. By this process we can find Δ (see Figure 2.3).

Using the process above, we can find the relative maximum for a given value of Ω_R. However, we would also like to maximize the probability of excitation to be 1. Using Equation 2.5 we want to set $\Omega_R t$ to π. This maximizes the probability of finding our atoms in the excited state because when $\Omega_R t = \pi$, $P_{|2\rangle}(t) = 1$, so

$$T_{pulse} = \frac{\pi}{\Omega_R}. \tag{2.6}$$

As a reminder, based on Equations 2.1b and 2.4d, Ω_R is dependent on coupling strength of the transition and laser amplitude.

The experimental process to determine the resonance frequency begins first by optically pumping the atoms into state $|1\rangle$. The optical pumping is accomplished by turning on a single laser field tuned on-resonance with the $|2\rangle \rightarrow |3\rangle$ transition. Through the process of spontaneous emission, the atom either decays back into state $|2\rangle$, in which case it gets re-excited to state $|3\rangle$, or it drops into state $|1\rangle$, where it remains because the single laser field is far off resonance with the $|1\rangle \rightarrow |3\rangle$ transition. The optical pumping light is switched off and we begin the Raman process. This process involves applying a pulse of light of temporal duration T_{pulse} for a given value for δ_{2p}, measuring the number of atoms in the excited state then repeating with a different value of δ_{2p} and so on. To properly describe this experimental procedure, we must use the full probability equation, Equation 2.4c, and a large detuning. It is important to keep in mind that T_{pulse} does not change during this process.

After the Raman pulse, we apply the detection pulse. This pulse is designed to measure atoms in the upper ground state by being tuned to the $|2\rangle \rightarrow |3\rangle$ transition. Nominally, the detection laser can be the same laser as the optical pumping laser. This laser excites the atoms in state $|2\rangle$ with a probability of 1 (see Equation 2.4c). When these atoms get excited, they fluoresce, and the amount of fluorescence is proportional to the number of atoms in state $|2\rangle$. As the Raman laser two-photon detuning is scanned, the number of atoms in the excited state changes. By graphing the data and comparing to the frequency of the laser and amplitude of our measurement of the excited state $|2\rangle$ atoms, we can determine our hyperfine splitting frequency, Δ. This process is called Raman spectroscopy.

Figure 2.4 shows the probability of atoms being excited as a function of detuning. As previously discussed, it is very important to have the detection laser tuned perfectly on resonance. The probability of exciting the atoms falls off drastically as it is tuned slightly off resonance, which effects the overall accuracy of the Raman measurements.

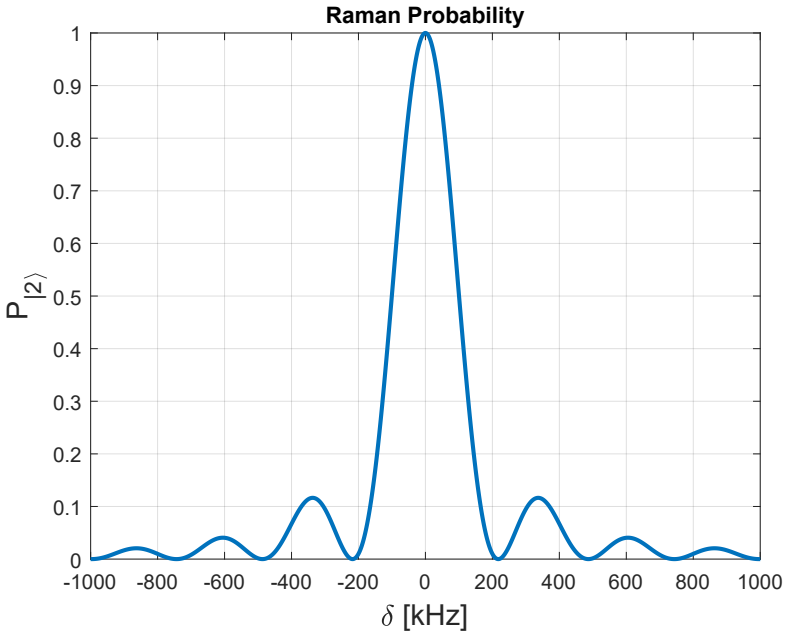

Figure 2.4. Probability of atoms in the excited state ($P_{|2\rangle}$) as a function of detuning which results in the standard Raman spectrum. $T_{pulse} = 25\ \mu s$

At this point, we have determined the value of Δ and know how to tune the Raman laser to zero two-photon detuning. We also now know the value of the Rabi frequency Ω and pulse time T_{pulse} required for a π pulse. Armed with this knowledge, we move on to Ramsey spectroscopy.

2.4 Ramsey Spectroscopy

Ramsey spectroscopy is a method of spectroscopy named after Norman Ramsey, who first proposed it [26]–[28] and who later won the Nobel prize for the idea [29], [30].

The idea behind Ramsey spectroscopy emerged due to attempts being made to improve on the Raman spectroscopy technique in molecular beams for clock applications. As we see

in Figure 2.4, the Raman curve resulting from plotting Equation 2.4c as a function of δ_{2p} is a sync function, which is the Fourier transform of a square pulse (which is what is used in the experiments). The center of that Fourier transformed pulse is the measurement of Δ. The width of the Fourier transform curve is proportional to $\frac{1}{T}$. To narrow the peak and make the measurement for Δ more accurate, we must increase the time of the Raman π-pulse. It is theoretically possible to apply a longer pulse. However, experimentally this was a challenge. At the time, these Raman experiments were using atom beams, which take up a lot of physical space (due to the speed of the atoms). In order to apply a longer pulse, larger optics that would take up more space would be required. In addition to the added space requirement, it was exponentially more difficult to create a uniform laser field, electric field, magnetic field, etc., all of which affect the final measurement accuracy [31].

Ramsey's solution to the problem discussed in the previous paragraph uses two short pulses, each of which constitutes a $\pi/2$ pulse separated by a long time where the atoms evolve in the dark. Under the right conditions, the two $\pi/2$ pulses combined can be equivalent to a single π pulse, but in general, the two pulses cause interference fringes that can be used to better localize the peak of the Raman transition. This dark evolution time is denoted by T_{evol}. A long T_{evol} replaces the need for a long pulse T_{pulse} and solves the experimental challenges described above. Ramsey spectroscopy determines Δ with better accuracy than Raman spectroscopy and is also a building block for atom interferometry.

Figure 2.5 depicts in time what a Ramsey pulse sequence looks like. The atoms are optically prepared in exactly the same fashion as the state preparation in Raman spectroscopy. The first $\pi/2$ pulse creates a coherent superposition of the two states (in principle, equally weighed). In quantum mechanics, the superposition of states means that the atom will sometimes behave as if it is in the ground state and sometimes as if it is in the excited state. This is *not* an average between the ground and excited states. After the atom passes through the first $\pi/2$-pulse it then travels through an interaction zone where the atom picks up a phase factor. This phase factor contains information about the potentials the atoms are experiencing (e.g., gravitational, rotational). This effect will be discussed more in Chapter 3.

The second $\pi/2$-pulse interacts with the atom in the same way as the first $\pi/2$-pulse, which means there are still two possible outcomes for each atom. After the second $\pi/2$-pulse there are four outcomes: the atom will

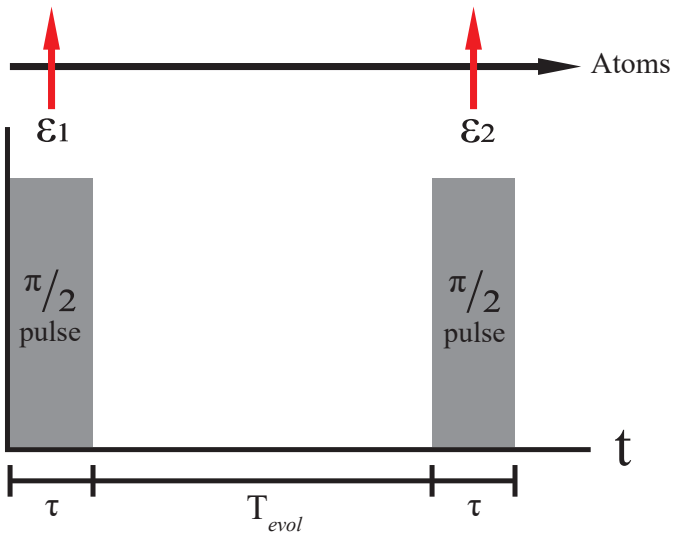

Figure 2.5. Ramsey spectroscopy temporal pulse sequence.

- get excited by the first pulse and remain excited after the second pulse,
- get excited by the first pulse and return to the ground state after the second pulse,
- remain in the ground state after the first pulse and remain in the ground state after the second pulse,
- remain in the ground state after the first pulse and get excited after the second pulse.

A detection laser is used to measure the number of atoms that are in the excited state in the same manner as was described for Raman spectroscopy. The probability of the atoms in the excited state after passing through a Ramsey interferometer is determined by the following

iterations on the wave function:

$$\begin{aligned}
\text{Initial wave function: } |\Psi\rangle &= |g\rangle \\
\text{After first } \frac{\pi}{2} \text{ pulse } |\Psi\rangle &= \frac{1}{\sqrt{2}}(|g\rangle + i\,|e\rangle) \\
\text{After free evolution time } T_{evol}\,|\Psi\rangle &= \frac{1}{\sqrt{2}}(|g\rangle + ie^{i\delta T}\,|e\rangle) \\
\text{After second } \frac{\pi}{2} \text{ pulse } |\Psi\rangle &= \frac{1}{\sqrt{2}}\left(\frac{|g\rangle + i\,|e\rangle}{\sqrt{2}} + ie^{i\delta T}\frac{i\,|g\rangle + |e\rangle}{\sqrt{2}}\right) \\
\text{Projection against } \langle e|\,\langle e|\Psi\rangle &= \frac{1}{2}(i + ie^{i\delta T}) \\
\text{Probability } P &= |\,\langle e|\Psi\rangle\,|^2 = \frac{1}{2}(1 + e^{i\delta T})\frac{1}{2}(1 + e^{i\delta T}) \\
P &= \frac{1}{4}(1 + 1 + 2\cos\delta T) \\
P &= \frac{1}{2}\,(1 + \cos\delta T) \qquad (2.7)
\end{aligned}$$

After the second $\pi/2$-pulse there are a certain number of atoms that are excited and a certain number of atoms that are in the ground state as given by Equation 2.7. Just as in the Raman process, we turn on a laser to measure the atoms in the excited state. In this thesis, we explore the use of squeezed light as a detection field in atom interferometry. To do this, we use the Ramsey process as the basic interferometer in which to explore the utility of this arrangement.

The detection process is a critical piece of Ramsey spectroscopy. After the atoms pass through a Ramsey interferometer, a laser is directed on those atoms and they fluoresce. The number of photons that are detected due to the fluorescence is based on the total number of atoms, how fast the atoms decay (spontaneous emission rate), and the number of atoms in the excited state due to the Ramsey interferometer. This is given by [32]

$$n_p = \alpha g N 2\beta \frac{\frac{1}{4}\frac{\Omega^2}{\beta^2}}{\frac{1}{2}\frac{\Omega^2}{\beta^2} + 1 + \frac{\delta^2}{\beta^2}}, \qquad (2.8)$$

where 2β is the excited state decay rate. For ^{85}Rb, this quantity is $2\pi(3 \times 10^6)$Hz [33]. However, we measure a voltage to determine the number of photons per second. To convert

photons per second into a voltage, we have

$$V = RS\hbar\omega_L n_p, \tag{2.9}$$

where n_p is the number of detected photons per second, ω_L is the laser frequency, R is the resistance used to convert the current detector into a voltage source, and S is the sensitivity of the detector in $Amps/Watt$. If we recall that the Rabi frequency, Ω, is proportional to the square root of the laser power, then we can note that if the laser has intensity noise, the same number of atoms every time we will have a different number of detected photons because fluctuations in laser power lead to fluctuations in n_p. As mentioned earlier, the laser suffers from both technical noise and quantum noise. However, each noise source impacts the measured voltage signal in the same way. The way to make V more stable is to use a detection beam that is less noisy than that of a standard beam (e.g., squeezed light).

CHAPTER 3:
Theory

3.1 Calculations

In this chapter, we present a fully quantum treatment of an atom interacting with two light fields. We develop a general framework for the calculations that can be used for any quantum state of light. We then apply the resulting equations to coherent states of light, which typically are used to mimic the behavior of classical laser fields. We then apply the same equations to squeezed light to begin to explore the utility of using squeezed light in Raman and Ramsey spectroscopy. We begin by establishing the Hamiltonian in the form [18], [20]:

$$\hat{\mathcal{H}} = \hat{\mathcal{H}}_0 + \hat{\mathcal{H}}_I, \tag{3.1a}$$

where $\hat{\mathcal{H}}_0$ is the bare Hamiltonian and $\hat{\mathcal{H}}_I$ is the interaction Hamiltonian.

$$\hat{\mathcal{H}}_O = \hbar\omega_0 \hat{b}^\dagger \hat{b} + \hbar\omega_L \hat{a}^\dagger \hat{a} \tag{3.1b}$$

$$\hat{\mathcal{H}}_I = -\hat{\boldsymbol{\mu}} \cdot \hat{\boldsymbol{E}}(\boldsymbol{r}, t). \tag{3.1c}$$

Here, ω_0 is the atomic transition frequency, ω_L is the laser frequency, $\hat{b}^\dagger$ and $\hat{b}$ are the atomic raising and lowering operators ($|2\rangle\langle 1|$ and $|1\rangle\langle 2|$, respectively), and $\hat{a}^\dagger$ and $\hat{a}$ are the harmonic oscillator raising and lowering operators (used to model the single mode laser field). $\hat{\boldsymbol{\mu}}$ is the atomic dipole operator and $\hat{\boldsymbol{E}}(\boldsymbol{r}, t)$ is the laser electric field. The dipole operator $\hat{\boldsymbol{\mu}}$ can be written in terms of the atomic raising and lowering operators, shown in [19] as

$$\hat{\boldsymbol{\mu}} = \boldsymbol{\mu}_{12}\hat{b} + \boldsymbol{\mu}_{12}^* \hat{b}^\dagger. \tag{3.2}$$

In most textbook cases of the interaction of a single atom with a single mode field, the electric field is treated as a classical field and hence $\boldsymbol{E}(\boldsymbol{r}, t)$ is not an operator but a c-

number [18], [20]. However, we are interested in the effect of squeezed light (which is a quantum effect) on the atom and so we need to also treat the electric field as an operator. As shown in [19], the quantum mechanical version of the electric field, in general, can be written as

$$\hat{\boldsymbol{E}}(\boldsymbol{r},t) = \sum_{\omega_{\boldsymbol{k},s}} \ell(\omega_{\boldsymbol{k},s})\hat{a}_{\omega_{\boldsymbol{k},s}}\boldsymbol{\epsilon}_{\omega_{\boldsymbol{k},s}} e^{\imath \boldsymbol{k}\cdot\boldsymbol{r}} + h.c.\,, \tag{3.3}$$

where $h.c.$ denoted the *hermitian conjugate*. In Equation 3.3, $\hat{a}_{\omega_{\boldsymbol{k},s}}$ is again the harmonic oscillator lowering operator, where we emphasize that an operator is required for *each* mode $\boldsymbol{k}$ of the electric field and for each of the two polarization states s. Also, $\boldsymbol{\epsilon}_{\omega_{\boldsymbol{k},s}}$ is the polarization vector associated with the $(\boldsymbol{k}, s)$ mode. Finally, $\ell(\omega_{\omega_{\boldsymbol{k},s}})$ is a frequency-dependent amplitude, whose form is not critical to our calculations included here for completeness [19],

$$\ell(\omega_{\omega_{\boldsymbol{k},s}}) = \frac{i}{L^{3/2}}\left(\frac{\hbar\omega}{2\varepsilon_0}\right)^{1/2}, \tag{3.4}$$

where ε_0 is the permittivity of free space and L is the length of a quantization box (to be taken to infinity at the end of the calculations). We can greatly simplify the equations by assuming a single-mode field of single polarization interacting with an atom located at the origin ($\boldsymbol{r} = 0$). Thus, the electric field can be written as

$$\hat{\boldsymbol{E}}(0,t) = \ell(\omega)\hat{a}\boldsymbol{\epsilon}_L + h.c., \tag{3.5}$$

where we denote the single polarization vector of the field by $\boldsymbol{\epsilon}_L$.

From Equation 3.1c, we see that we need to calculate the dot product $\hat{\boldsymbol{\mu}} \cdot \boldsymbol{E}(0,t)$, which is given by

$$\begin{aligned}
\hat{\boldsymbol{\mu}} \cdot \boldsymbol{E}(0,t) &= \left(\boldsymbol{\mu}_{12}\hat{b} + c.c.\right) \cdot \left(\ell(\omega)\hat{a}\boldsymbol{\epsilon}_L + c.c.\right) \\
&= \left(\boldsymbol{\mu}_{12} \cdot \boldsymbol{\epsilon}_L\right)\ell(\omega)\hat{b}\hat{a} + \left(\boldsymbol{\mu}_{12}^* \cdot \boldsymbol{\epsilon}_L^*\right)\ell^*(\omega)\hat{a}^\dagger\hat{b}^\dagger \\
&\qquad + \left(\boldsymbol{\mu}_{12} \cdot \boldsymbol{\epsilon}_L^*\right)\ell^*(\omega)\hat{a}^\dagger\hat{b} + \left(\boldsymbol{\mu}_{12}^* \cdot \boldsymbol{\epsilon}_L\right)\ell(\omega)\hat{a}\hat{b}^\dagger.
\end{aligned} \tag{3.6a}$$

The first two terms in Equation 3.6a eventually integrate away to zero under the rotating

wave approximation [18]. This gives us

$$\hat{\boldsymbol{\mu}} \cdot \boldsymbol{E} = \left(\boldsymbol{\mu}_{12} \cdot \boldsymbol{\epsilon}_L^*\right) \ell^*(\omega) \hat{a}^\dagger \hat{b} + \left(\boldsymbol{\mu}_{12}^* \cdot \boldsymbol{\epsilon}_L\right) \ell(\omega) \hat{a} \hat{b}^\dagger. \tag{3.6b}$$

In this form, Equation 3.6b has a simple interpretation. The first term describes the "destruction" of the atomic excitation by the atomic lowering operator ($\hat{b}$) with the simultaneous creation of a photon ($\hat{a}^\dagger$). The second term describes the absorption and hence destruction of a photon by the photon annihilation operator ($\hat{a}$) and the simultaneous excitation of the atom through the atomic excitation operator ($\hat{b}^\dagger$).

At this stage, we follow convention [18] and define a coupling constant g as

$$\mathrm{g} \equiv \frac{2\left(\boldsymbol{\mu}_{12}^* \cdot \boldsymbol{\epsilon}_L\right)}{\hbar} \ell(\omega) \tag{3.6c}$$

so that in terms of the coupling constant, the full Hamiltonian in the Schrodinger picture within the rotating wave approximation becomes

$$\hat{\mathcal{H}} = \hbar\omega_0 \hat{b}^\dagger \hat{b} - \frac{1}{2}\hbar g^* \hat{a}^\dagger \hat{b} - \frac{1}{2}\hbar g \hat{a} \hat{b}^\dagger. \tag{3.6d}$$

Now, we have derived the full Hamiltonian for the interaction of a single atom with a single-mode electric field. In order to further simplify the calculations, we now move into the interaction picture. The initial Schrodinger equation is [18, Ch. 5, p. 155]

$$\hat{\mathcal{H}} \left|\psi(t)\right\rangle = i\hbar \frac{d}{dt} \left|\psi(t)\right\rangle. \tag{3.7}$$

When there is no interaction, the Schrodinger equation can be written as

$$\hat{\mathcal{H}}_0 \left|\psi(t)\right\rangle = i\hbar \frac{d}{dt} \left|\psi(t)\right\rangle, \tag{3.8}$$

which, since the bare Hamiltonian is time-independent, has the solution

$$\left|\psi(t)\right\rangle = e^{-\frac{i}{\hbar}\hat{\mathcal{H}}_0 t} \left|\psi(0)\right\rangle. \tag{3.9}$$

To transform the wave function into the interaction picture, we define a unitary operator

$\hat{U}(t)$ by

$$\hat{U}(t) = e^{\frac{-i}{\hbar}\hat{\mathcal{H}}_0 t}, \tag{3.10}$$

which satisfies the unitarity condition $\hat{U}^\dagger(t)\hat{U}(t) = 1$ by inspection. If we denote the wave function that is transformed in the interaction picture by $\left|\tilde{\psi}(t)\right\rangle$ (and indeed, throughout this section, anything with a tilde above it denotes the interaction picture), then we can write

$$\left|\tilde{\psi}(t)\right\rangle = \hat{U}^\dagger(t)\left|\psi(t)\right\rangle. \tag{3.11}$$

So far, all we have done is applied an "arbitrary" transformation, which is unitary, to the original wave function. We will now see that this transformation leads to a new Schrodinger-type equation which, is dependent only on the interaction portion of the Hamiltonian; hence, we call this the interaction picture. We can substitute into Equation 3.11 (after inverting it) into Equation 3.7 to get

$$\begin{aligned}
\left(\hat{\mathcal{H}}_0 + \hat{\mathcal{H}}_I\right)\left|\psi(t)\right\rangle &= i\hbar\frac{d}{dt}\left|\psi(t)\right\rangle \\
\left(\hat{\mathcal{H}}_0 + \hat{\mathcal{H}}_I\right)\hat{U}(t)\left|\tilde{\psi}(t)\right\rangle &= i\hbar\frac{d}{dt}\hat{U}(t)\left|\tilde{\psi}(t)\right\rangle \\
\hat{\mathcal{H}}_0\hat{U}(t)\left|\psi(t)\right\rangle + \hat{\mathcal{H}}_I\hat{U}(t)\left|\psi(t)\right\rangle &= i\hbar\left(\hat{U}(t)\frac{d}{dt}\left|\psi(t)\right\rangle + \frac{d\hat{U}(t)}{dt}\left|\psi(t)\right\rangle\right),
\end{aligned} \tag{3.12}$$

where we have

$$\begin{aligned}
\hat{U}(t) &= e^{\frac{-i}{\hbar}\hat{\mathcal{H}}_0 t} \\
\frac{d\hat{U}(t)}{dt} &= \frac{-i}{\hbar}\hat{\mathcal{H}}_0 e^{\frac{-i}{\hbar}\hat{\mathcal{H}}_0 t} = \frac{-i}{\hbar}\hat{\mathcal{H}}_0\hat{U}(t),
\end{aligned} \tag{3.13}$$

and we note $\left[\hat{\mathcal{H}}_0, \hat{U}(t)\right] = 0$ and are left with

$$\begin{aligned}
\hat{\mathcal{H}}_0\hat{U}(t)\left|\psi(t)\right\rangle + \hat{\mathcal{H}}_I\hat{U}(t)\left|\psi(t)\right\rangle &= i\hbar\hat{U}(t)\frac{d}{dt}\left|\psi(t)\right\rangle + \hat{\mathcal{H}}_0\hat{U}(t)\left|\psi(t)\right\rangle \\
\hat{\mathcal{H}}_I\hat{U}(t)\left|\psi(t)\right\rangle &= i\hbar\hat{U}(t)\frac{d}{dt}\left|\psi(t)\right\rangle \\
\hat{U}^\dagger\hat{\mathcal{H}}_I\hat{U}\left|\psi(t)\right\rangle &= i\hbar\frac{d}{dt}\left|\psi(t)\right\rangle \\
\hat{\tilde{\mathcal{H}}}_I(t)\left|\psi(t)\right\rangle &= i\hbar\frac{d}{dt}\left|\psi(t)\right\rangle, \qquad (3.14)
\end{aligned}$$

where we have defined the interaction Hamiltonian *in the interaction picture* by

$$\hat{\tilde{\mathcal{H}}}_I(t) = \hat{U}^\dagger(t)\hat{\mathcal{H}}_I\hat{U}(t). \qquad (3.15)$$

Examining Equation 3.14, we see it looks very much like the original Schrodinger equation (Equation 3.7), but with the Hamiltonian being given only by the interaction Hamiltonian. From this, we determine that the wave function in the Interaction picture only depends on the $\hat{\mathcal{H}}_I$ term and no $\hat{\mathcal{H}}_0$ term. The dependence on $\hat{\mathcal{H}}_I$ only means as we continue on in our discussion we can drop the $\hat{\mathcal{H}}_0$ term entirely.

In order to arrive at a Schrodinger-like equation in the transformed basis, we needed to define the transformed operator $\hat{\tilde{\mathcal{H}}}_I$ by Equation 3.15. Using this as a guide, we can consider the transformation of any generic operator $\hat{A}$ from the Schrodinger picture to the Interaction picture and consider the time evolution of the operator in the interaction picture

$$\begin{aligned}
\hat{\tilde{A}}(t) &= \hat{U}^\dagger(t)\hat{A}(t)\hat{U}(t) \\
\frac{d}{dt}\tilde{A}(t) &= \frac{d\hat{U}^\dagger(t)}{dt}\hat{A}(t)\hat{U}(t) + \hat{U}^\dagger(t)\frac{d\hat{A}(t)}{dt}\hat{U}(t) + \hat{U}^\dagger(t)\hat{A}(t)\frac{d\hat{U}(t)}{dt} \\
\frac{d}{dt}\hat{\tilde{A}}(t) &= \hat{U}^\dagger(t)\hat{A}(t)\left(-\frac{i}{\hbar}\hat{H}_0\hat{U}(t)\right) + \frac{i}{\hbar}\hat{H}_0\hat{U}^\dagger(t)\hat{A}(t)\hat{U}(t) \\
&= -\frac{i}{\hbar}\left(\hat{U}^\dagger(t)\hat{A}(t)\hat{U}(t)\hat{\mathcal{H}}_0 - \hat{\mathcal{H}}_0\hat{U}^\dagger(t)\hat{A}(t)\hat{U}(t)\right) \\
&= \frac{i}{\hbar}\left[\hat{\mathcal{H}}_0, \hat{\tilde{A}}(t)\right], \qquad (3.16a)
\end{aligned}$$

where, in our case, the operators we will be dealing with are explicitly not time-dependent in the Schrodinger picture and so, we take $d\hat{A}(t)/dt = 0$.

Specifically, the transformations for the field operator $\hat{a}$ and the atomic operator $\hat{b}$ are as follows:

$$\begin{aligned}\frac{d\hat{\tilde{a}}}{dt} &= \frac{i}{\hbar}\left[\hat{\mathcal{H}}_0, \hat{a}\right] \\ &= \frac{i}{\hbar}\left[\hbar\omega_L n, \hat{a}\right] \\ &= -i\omega_L \hat{a}.\end{aligned}$$

Integrating, we obtain

$$\begin{aligned}\hat{\tilde{a}}(t) &= \hat{a}(0)e^{-i\omega_L t} \\ \hat{\tilde{a}}(t) &= \hat{a}_s e^{-i\omega_L t}\end{aligned} \tag{3.17a}$$

where $\hat{a}_s$ in the Schrodinger picture coincides with $\hat{a}(0)$. Similarly, we can derive an expression for the atomic operator $\hat{b}$ as

$$\begin{aligned}\frac{d\hat{\tilde{b}}}{dt} &= \frac{i}{\hbar}\left[\hbar\omega_0 \hat{b}^\dagger \hat{b}, \hat{b}\right] \\ &= i\omega_0 \left(|2\rangle\langle 2|1\rangle\langle 2| - |1\rangle\langle 2|2\rangle\langle 2|\right) \\ &= -i\omega_0 \hat{b}.\end{aligned}$$

Again, integrating, we obtain

$$\begin{aligned}\hat{\tilde{b}}(t) &= \hat{b}(0)e^{-i\omega_0 t} \\ &= \hat{b}_s e^{-i\omega_0 t}.\end{aligned} \tag{3.17b}$$

Using Equations 3.17a and 3.17b, we can now transform the Hamiltonian from the

Schrodinger picture to the Interaction picture

$$\begin{aligned}\hat{\hat{\mathcal{H}}}_I &= -\frac{1}{2}\hbar\Omega^*\hat{a}^\dagger\hat{b} - \frac{1}{2}\hbar\Omega\hat{a}\hat{b}^\dagger \\ &= -\frac{1}{2}\hbar g^*\hat{\hat{a}}^\dagger e^{-i\omega_L t}\hat{\hat{b}}e^{i\omega_0 t} - \frac{1}{2}\hbar g\hat{\hat{a}}e^{i\omega_L t}\hat{\hat{b}}^\dagger e^{-i\omega_0 t} \\ &= -\frac{1}{2}\hbar g^*\hat{\hat{a}}^\dagger\hat{\hat{b}}e^{-i\delta t} - \frac{1}{2}\hbar g\hat{\hat{a}}\hat{\hat{b}}^\dagger e^{i\delta t}, \end{aligned} \tag{3.18}$$

where $\delta = \omega_L - \omega_0$. We have now derived the interaction Hamiltonian in the interaction picture that describes the interaction of a single mode laser field with a single, two-level atom.

We now turn to the description of the actual experiment. While Raman spectroscopy only requires one pulse, we need to account for the two pulses the atoms experience during Ramsey spectroscopy. Figure 2.5 depicts these two pulses that occur during Ramsey spectroscopy on a timeline. Accounting for both of the interactions in our final Hamiltonian can be done by judicious use of the Heaviside step function. The Heaviside step function is defined as

$$\theta(x) = \begin{cases} 0 & x < 0 \\ 1 & x \geq 1. \end{cases} \tag{3.19}$$

Since we start at the origin, the first pulse starts at $t = 0$, and lasts for $t = \tau$. The first $\pi/2$ pulse interacts with the atom from $t = 0$ to $t = \tau$. We want the pulse on at $t = 0$, and off for $t > \tau$, or in other words $\theta(x) = 0$ when $t = \tau$. However, since $\theta(t)$ is always equal to 1, we can ignore it in the equation and thus the interaction due to the first pulse can then be written as

$$\hat{\mathcal{H}}_1(t)\theta(\tau - t), \tag{3.20}$$

where $\hat{\mathcal{H}}_1$ is the interaction given by Equation 3.18 for the first pulse. Now, we must add the Hamiltonian associated with the second pulse, which will also be a product of two step functions. We want the interaction to turn on when $t = T + \tau$, so the first step function can be written as $\theta(t - (T + \tau))$. This makes sense because when t is larger than $T + \tau$, x is positive which equates to $\theta(x) = 1$. Any time before that t will be less than $T + \tau$ which

means $\theta(x) = 0$. Next, we also want the laser to turn off at $t = T + 2\tau$. For this part, the step function can be written as $\theta(T + 2\tau - t)$. The product of these two step functions will give us the Hamiltonian associated with the second pulse. It is written as

$$\hat{\mathcal{H}}_2(t)\theta(t - (T + \tau))\theta(T + 2\tau - t), \tag{3.21}$$

where again $\hat{\mathcal{H}}_2$ is the interaction given by Equation 3.18 but for the second pulse. Combining these two associated step functions together from Equations 3.20 and 3.21 gives us the interaction Hamiltonian for Ramsey spectroscopy in the interaction picture,

$$\hat{\mathcal{H}}_1(t)\theta(\tau - t) + \hat{\mathcal{H}}_2(t)\theta(t - (T + \tau))\theta(T + 2\tau - t). \tag{3.22}$$

Now we can substitute in Equation 3.18 for $\hat{\mathcal{H}}_1$ and $\hat{\mathcal{H}}_2$ and we get

$$\begin{aligned}\hat{\tilde{\mathcal{H}}}_I(t) &= \left[-\frac{1}{2}\hbar g^* \hat{\tilde{a}}^\dagger \hat{\tilde{b}} e^{-i\delta t} - \frac{1}{2}\hbar g \hat{\tilde{a}} \hat{\tilde{b}}^\dagger e^{i\delta t}\right]\theta(\tau - t) \\ &\quad - \left[\frac{1}{2}\hbar g^* \hat{\tilde{a}}^\dagger \hat{\tilde{b}} e^{-i\delta t} - \frac{1}{2}\hbar g \hat{\tilde{a}} \hat{\tilde{b}}^\dagger e^{i\delta t}\right]\theta(t - (T + \tau))\theta(T + 2\tau - t).\end{aligned} \tag{3.23}$$

The formal solution of 3.14 is

$$|\psi(t)\rangle = e^{\frac{i}{\hbar}\int_0^t \hat{\mathcal{H}}(t)dt}\,|\psi(0)\rangle\,, \tag{3.24}$$

where the exponential can be expanded in a Taylor series to provide the approximate solution

$$|\psi(t)\rangle = \left[1 - \frac{i}{\hbar}\int_0^t \hat{\tilde{\mathcal{H}}}_I(t')dt'\right]|\psi(0)\rangle\,; \tag{3.25}$$

therefore, our next step is to integrate Equation 3.23 over time.

$$\begin{aligned}
\int_0^{\tau} \hat{\tilde{\mathcal{H}}}_I(t')dt' + \int_{T+\tau}^{T+2\tau} \hat{\tilde{\mathcal{H}}}_I(t')dt' &= \left[-\frac{1}{2}\hbar g^* \hat{\tilde{a}}^\dagger \hat{\tilde{b}} \int_0^{\tau} e^{-i\delta t'} dt' - \frac{1}{2}\hbar g \hat{\tilde{a}} \hat{\tilde{b}}^\dagger \int_0^{\tau} e^{i\delta t'} dt'\right] \\
&\quad - \left[\frac{1}{2}\hbar g^* \hat{\tilde{a}}^\dagger \hat{\tilde{b}} \int_{T+\tau}^{T+2\tau} e^{-i\delta t'} dt' - \frac{1}{2}\hbar g \hat{\tilde{a}} \hat{\tilde{b}}^\dagger \int_{T+\tau}^{T+2\tau} e^{i\delta t'} dt'\right] \\
&= \left[-\frac{1}{2}\hbar g^* \hat{\tilde{a}}^\dagger \hat{\tilde{b}} \frac{e^{-i\delta\tau} - 1}{-i\delta} - \frac{1}{2}\hbar g \hat{\tilde{a}} \hat{\tilde{b}}^\dagger \frac{e^{i\delta\tau} - 1}{i\delta}\right] \\
&\quad - \left[\frac{1}{2}\hbar g^* \hat{\tilde{a}}^\dagger \hat{\tilde{b}} \frac{e^{-i\delta(T+2\tau)} - e^{-i\delta(T+\tau)}}{i\delta} - \right. \\
&\quad \left. \frac{1}{2}\hbar g \hat{\tilde{a}} \hat{\tilde{b}}^\dagger \frac{e^{i\delta(T+2\tau)} - e^{i\delta(T+\tau)}}{-i\delta}\right]. \qquad (3.26)
\end{aligned}$$

From here, we simplify and set

$$f(\tau) = \frac{e^{i\delta\tau} - 1}{i\delta}. \qquad (3.27)$$

The resulting integration of the interaction Hamiltonian becomes

$$\begin{aligned}
\int \hat{\tilde{\mathcal{H}}}_I(t')dt' &= -\frac{1}{2}\hbar g^* \hat{\tilde{a}}^\dagger \hat{\tilde{b}} f^*(\tau) - \frac{1}{2}\hbar g \hat{\tilde{a}} \hat{\tilde{b}}^\dagger f(\tau) - \frac{1}{2}\hbar g^* \hat{\tilde{a}}^\dagger \hat{\tilde{b}} \left(\frac{e^{-i\delta(T+2\tau)} - e^{-i\delta(T+\tau)}}{-i\delta}\right) \\
&\quad -\frac{1}{2}\hbar g \hat{\tilde{a}} \hat{\tilde{b}}^\dagger \left(\frac{e^{i\delta(T+2\tau)} - e^{i\delta(T+\tau)}}{i\delta}\right) \\
&= -\frac{1}{2}\hbar g^* \hat{\tilde{a}}^\dagger \hat{\tilde{b}} f^*(\tau) - \frac{1}{2}\hbar g \hat{\tilde{a}} \hat{\tilde{b}}^\dagger f(\tau) \\
&\quad -\frac{1}{2}\hbar g^* \hat{\tilde{a}}^\dagger \hat{\tilde{b}} \left(\frac{e^{-i\delta\tau} - 1}{-i\delta}\right) e^{-i\delta(T+\tau)} - \frac{1}{2}\hbar g \hat{\tilde{a}} \hat{\tilde{b}}^\dagger \left(\frac{e^{i\delta\tau)} - 1}{i\delta}\right) e^{i\delta(T+\tau)} \\
&= -\frac{1}{2}\hbar g^* \hat{\tilde{a}}^\dagger \hat{\tilde{b}} f^*(\tau) - \frac{1}{2}\hbar g \hat{\tilde{a}} \hat{\tilde{b}}^\dagger f(\tau) \\
&\quad -\frac{1}{2}\hbar g^* \hat{\tilde{a}}^\dagger \hat{\tilde{b}} f^*(\tau) e^{-i\delta(T+\tau)} - \frac{1}{2}\hbar g \hat{\tilde{a}} \hat{\tilde{b}}^\dagger f(\tau) e^{i\delta(T+\tau)}. \qquad (3.28)
\end{aligned}$$

So far, we have ignored the fact that the two different $\pi/2$ pulses come from two different modes. We take this into account by distinguishing between the two modes in our field

operator $\hat{\hat{a}}$ and $\hat{\hat{a}}^\dagger$.

$$\begin{aligned}\int \hat{\hat{\mathcal{H}}}_I(t')dt' &= -\frac{1}{2}\hbar g^* \hat{\hat{a}}_1^\dagger \hat{\hat{b}} f^*(\tau) - \frac{1}{2}\hbar g \hat{\hat{a}}_1 \hat{\hat{b}}^\dagger f(\tau) \\ &\quad -\frac{1}{2}\hbar g^* \hat{\hat{a}}_2^\dagger \hat{\hat{b}} f^*(\tau) e^{-i\delta(T+\tau)} - \frac{1}{2}\hbar g \hat{\hat{a}}_2 \hat{\hat{b}}^\dagger f(\tau) e^{i\delta(T+\tau)}. \end{aligned} \quad (3.29)$$

Now, we define the initial state of the system. For this, we define the atom to be in the ground state with the two quantum fields, denoted by $|\phi_1\rangle$ and $|\phi_2\rangle$, which are unspecified as of yet. Thus the initial state of the wave function is

$$|\psi(0)\rangle = |1\rangle\,|\phi_1\rangle\,|\phi_2\rangle\,. \quad (3.30)$$

With our initial state defined, our wave function now becomes

$$\begin{aligned}|\psi(t)\rangle &= \left(1 - \frac{i}{\hbar}\int_0^t \hat{\hat{\mathcal{H}}}_I(t')dt'\right)|\psi(0)\rangle \\ &= \left(1 - \frac{i}{\hbar}\int_0^{t_1} \hat{\hat{\mathcal{H}}}_I(t')dt' - \frac{i}{\hbar}\int_{t_1}^{2\tau+t} \hat{\hat{\mathcal{H}}}_I(t')dt'\right)|\psi(0)\rangle \\ &= |\psi(0)\rangle + igf(\tau)\,|2\rangle\,\hat{\hat{a}}_1 + igf(\tau)\,|2\rangle\,|\phi_1(0)\rangle\left(\hat{\hat{a}}_2\,|\phi_2(0)\rangle\right)e^{i\delta(T+\tau)}. \end{aligned} \quad (3.31)$$

The experiment measures atoms in the excited state. We define the *measurement* operator as the projection operator into the excited state (e.g., $\hat{M} \equiv |e\rangle\langle e|$). Then, we find the expectation value of this operator with respect to the state $|\psi(t)\rangle$.

$$\begin{aligned}\hat{M}\,|\psi(t)\rangle &= igf(\tau)\,|e\rangle\,\hat{\hat{a}}_1\,|\phi_1(0)\rangle\,|\phi_2(0)\rangle + igf(\tau)e^{i\delta(T+\tau)}\,|e\rangle\,|\phi_1(0)\rangle\,\hat{\hat{a}}_2\,|\phi_2(0)\rangle \\ \langle\psi(t)|\hat{M}|\psi(t)\rangle &= \Big[\langle g|\,\langle\phi_1(0)|\,\langle\phi_2(0)| - ig^* f^*(\tau)\,\langle e|\,\langle\phi_1(0)|\,\hat{\hat{a}}_1^\dagger\,\langle\phi_2(0)| \\ &\qquad -ig^* f^*(\tau)\,\langle e|\,\langle\phi_1(0)|\,(\langle\phi_2(0)|\,\hat{\hat{a}}_2^\dagger)e^{-i\delta(T+\tau)}\Big] \\ &\qquad\qquad \Big[igf(\tau)\,|e\rangle\,\hat{\hat{a}}_1\,|\phi_1(0)\rangle\,|\phi_2(0)\rangle + igf(\tau)e^{i\delta(T+\tau)}\,|e\rangle\Big]\end{aligned}$$

Noting that $\langle \hat{M} \rangle \equiv \langle \psi(t) | \hat{M} | \psi(t) \rangle$, we have

$$\begin{aligned}
\langle \hat{M} \rangle &= |g|^2 |f(\tau)|^2 \langle \phi_1(0) | \hat{\tilde{a}}_1^\dagger \hat{a}_1 | \phi_1(0) \rangle + |g|^2 |f(\tau)|^2 \langle \phi_2(0) | \hat{\tilde{a}}_2^\dagger \hat{a}_2 | \phi_2(0) \rangle \\
&\quad + |g|^2 |f(\tau)|^2 \langle \phi_1(0) | \hat{\tilde{a}}_1^\dagger | \phi_1(0) \rangle \langle \phi_2(0) | \hat{\tilde{a}}_2 | \phi_2(0) \rangle e^{i\delta(T+\tau)} \\
&\quad + |g|^2 |f(\tau)|^2 \langle \phi_1(0) | \hat{\tilde{a}}_1 | \phi_1(0) \rangle \langle \phi_2(0) | \hat{\tilde{a}}_2^\dagger | \phi_2(0) \rangle e^{-i\delta(T+\tau)} \\
\langle \hat{M} \rangle &= |g|^2 |f(\tau)|^2 \Big[\langle \phi_1(0) | \hat{\tilde{a}}_1^\dagger \hat{a}_1 | \phi_1(0) \rangle + \langle \phi_2(0) | \hat{\tilde{a}}_2^\dagger \hat{\tilde{a}}_2 | \phi_2(0) \rangle \\
&\qquad + 2 | \langle \hat{\tilde{a}}_1^\dagger \rangle \langle \hat{\tilde{a}}_2 \rangle | \cos\left(\theta + \delta(T+\tau)\right) \Big]
\end{aligned} \tag{3.32}$$

Equation 3.32 is the general equation for the expectation value of the measurement operator for the case of the atom initiated in the ground state and the laser field unspecified. We can apply Equation 3.32 to the special case of coherent states. Later in this thesis, we will apply it to the case of squeezed states.

Now, consider the case of coherent states, which are eigenstates of the harmonic oscillator lowering operator, (i.e., $\hat{a} |\alpha\rangle = \alpha |\alpha\rangle$). Thus setting the initial states of the field, $|\phi_1(0)\rangle$ and $|\phi_2(0)\rangle$ to be the coherent states $|\alpha_1\rangle$ and $|\alpha_2\rangle$, respectively, we get

$$\langle \hat{M} \rangle = |g|^2 |f(\tau)|^2 \left[|\alpha_1|^2 + |\alpha_2|^2 + 2\alpha_1^* \alpha_2 \cos\left(\theta + \delta(T+\tau)\right) \right]. \tag{3.33}$$

This function is plotted in Figure 3.1 as a function of δ (recalling that $f(\tau)$ is also a function of δ). This result shows that our calculations recover the standard Ramsey interference plot.

Now that we have a model of the *measurement* operator, the next step is to model our noise. Noise is defined as

$$\langle \left(\Delta \hat{M}\right)^2 \rangle \equiv \langle \hat{M}^2 \rangle - \langle \hat{M} \rangle^2, \tag{3.34}$$

where we note

$$\hat{M}^2 = |e\rangle \langle e|e\rangle \langle e| = |e\rangle \langle e| = \hat{M}, \tag{3.35}$$

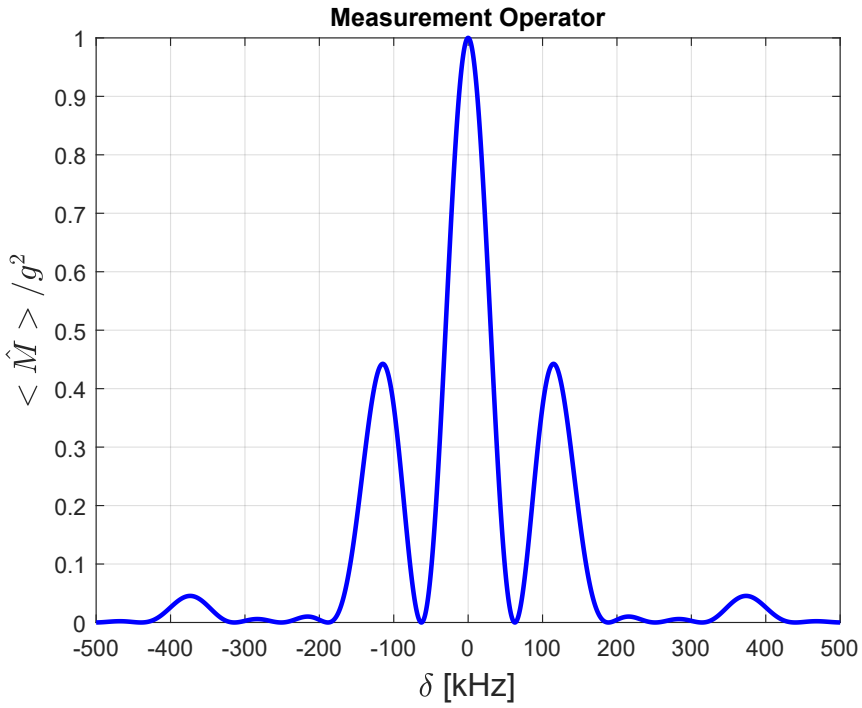

Figure 3.1. Normalized $\langle \hat{M} \rangle$ as a function of $f(\tau)$ for a coherent state. $\alpha_1 = \alpha_2 = 1, \tau = 25\mu s$

so we end up with

$$\begin{aligned} \langle (\Delta \hat{M})^2 \rangle &= \langle \hat{M} \rangle - \langle \hat{M} \rangle^2 \\ \langle (\Delta \hat{M})^2 \rangle &= \langle \hat{M} \rangle \left[1 - \langle \hat{M} \rangle \right] \\ \langle \Delta \hat{M} \rangle &= \sqrt{\langle \hat{M} \rangle \left[1 - \langle \hat{M} \rangle \right]}. \end{aligned} \tag{3.36}$$

This function is plotted in Figure 3.2 and will be used for comparison with similar plots for the squeezed states in the next section. This is the quantum noise of the measurement of the coherent state assuming a perfectly stable laser, with zero technical noise. A question to ask here is why does it matter to reduce our noise if the noise goes to zero on resonance and we conduct our experiments on resonance? In order to find the resonance frequency, we must scan the laser across a frequency range. The noise perfectly on resonance is zero, but as we can see from Figure 3.2 there is a lot of noise just slightly off resonance. As we scan to try

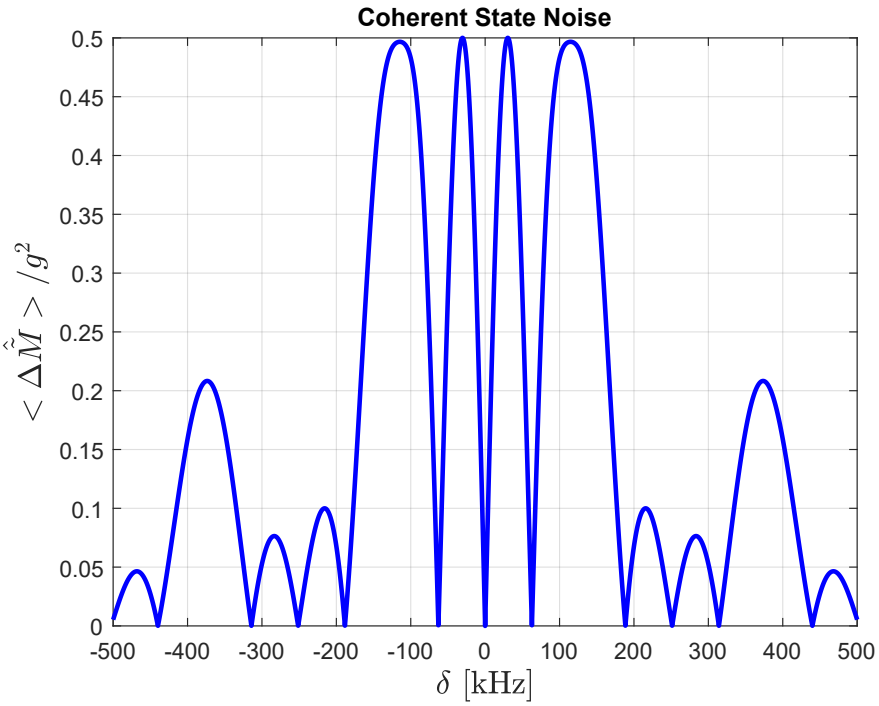

Figure 3.2. Normalized coherent state measurement noise as a function of detuning.

and find our signal peak (on resonance) we must scan over these areas of increased noise. If we can reduce the noise while off resonance, then we can increase the accuracy of our scan, and therefore increase the probability of finding our resonant frequency. The closer we are to being perfectly on resonance, the more likely we will have a probability of 1 when we excite atoms, as described previously for our Ramsey spectroscopy measurements.

3.2 Squeezed Light

Atom interferometer measurements are affected by the amount of noise from the incoming laser. In order to improve measurements from the interferometer we must find a way to reduce the amount of noise or at least manipulate it to our advantage. The incoming laser to an interferometer has a minimum amount of noise and this minimum threshold cannot be breached. However, it can be manipulated to produce squeezed light. Quantum noise in light is composed of two quadratures, which together cannot drop below the standard

quantum limit (SQL). We can make an analogy using simple math: $x * y = 2$. There are an infinite number of combinations of x and y that can equal 2; however, if x increases y must decrease, and vice versa, for the equation to still be true. Using squeezed light terminology, y would be considered in a squeezed state and have less signal variance than x. A quantum analogy is one of the quantum harmonic oscillator or electric field vectors of a light wave.

The equation for a single mode of the electric field is a special case of Equation 3.3; with the summation removed the interaction picture can be written as the following [19],

$$\hat{\boldsymbol{E}}(\boldsymbol{r},t) = l(\omega)\boldsymbol{\varepsilon}\left[\hat{a}e^{i(\boldsymbol{k}\cdot\boldsymbol{r}-\omega t} + \hat{a}^{\dagger}e^{-i(\boldsymbol{k}\cdot\boldsymbol{r}-\omega t}\right]. \tag{3.37}$$

We can define two new operators $\hat{Q}$ and $\hat{P}$

$$\left.\begin{aligned}\hat{Q} &= \hat{a}^{\dagger} + \hat{a} \\ \hat{P} &= i(\hat{a}^{\dagger} - \hat{a}),\end{aligned}\right\} \tag{3.38}$$

such that the field can be written as

$$\hat{\boldsymbol{E}}(\boldsymbol{r},t) = l(\omega)\boldsymbol{\varepsilon}\left[\hat{Q}\cos\left(\boldsymbol{k}\cdot\boldsymbol{r}-\omega t\right) - \hat{P}\sin\left(\boldsymbol{k}\cdot\boldsymbol{r}-\omega t\right)\right]. \tag{3.39}$$

With this form of the equation it is easy to see that the operators $\hat{Q}$ and $\hat{P}$ are the dimensionless canonical position and momentum operators for a harmonic oscillator. As such, they obey the usual well-known uncertainty relation [21], [22]

$$\langle(\Delta\hat{Q})^2\rangle^{1/2}\langle(\Delta\hat{P})^2\rangle^{1/2} \geq 1. \tag{3.40}$$

In terms of $\hat{a}$ and $\hat{a}^{\dagger}$ we get

$$\left|\langle(\Delta\hat{\hat{a}})\rangle\langle(\Delta\hat{\hat{a}^{\dagger}})\rangle\right| \geq \frac{1}{2}. \tag{3.41}$$

When light is squeezed, the Heisenberg uncertainty principle is still adhered to. However, variances of $\hat{Q}$ and $\hat{P}$ are unequal. For the Heisenberg uncertainty principle to still be true, one variance will have to decrease while the other increases [34]. The quadrature in which the variance is smaller is considered squeezed light.

Figure 3.3 shows the result of the measurement operator for a coherent state and for a particular type of squeezed light called a two-photon coherent state. A two-photon coherent state is the most widely studied squeezed state and so was chosen for our modeling [19]. This state is characterized by a squeezing parameter $z = re^{i\theta}$. We immediately noticed the loss of interference as exhibited by the shoulder in the plot around ±80kHz as compared to the zeros in the same spot for the coherent state. This is an undesirable result.

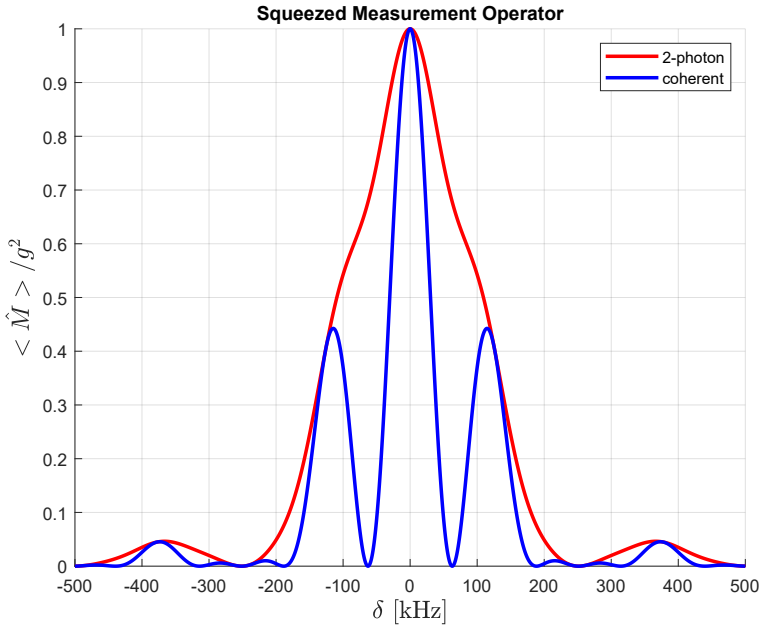

Figure 3.3. Measurement operator using squeezed states: $r_1 = r_2 = 1$, $\theta_1 = \theta_2 = 0$.

Here, we modeled two-photon squeezing with various parameters to identify the differences between the coherent state and squeezed state with respect to noise. As θ increases, we see something interesting happen. For our squeezed state, there is a dip in the noise around ±80kHz, much like for the coherent state, as θ increases from $\pi/2$ to π. The minimum of this dip occurs as $\theta = \pi$ and does not reach zero like in the coherent state. This is also not a desirable result, and is also expected. Since squeezed light is a gain process we expect there to be noise, but at this stage we have not analyzed all of the possible ways to exploit the squeezed state of light. What this model does not take into account is the two-mode correlation between the conjugate and probe beam that also is used in the FWM signal processing. More work needs to be done, but the modeling here lays a groundwork

for further analysis and experimentation of two-photon squeezed light (Figure 3.4 through Figure 3.6).

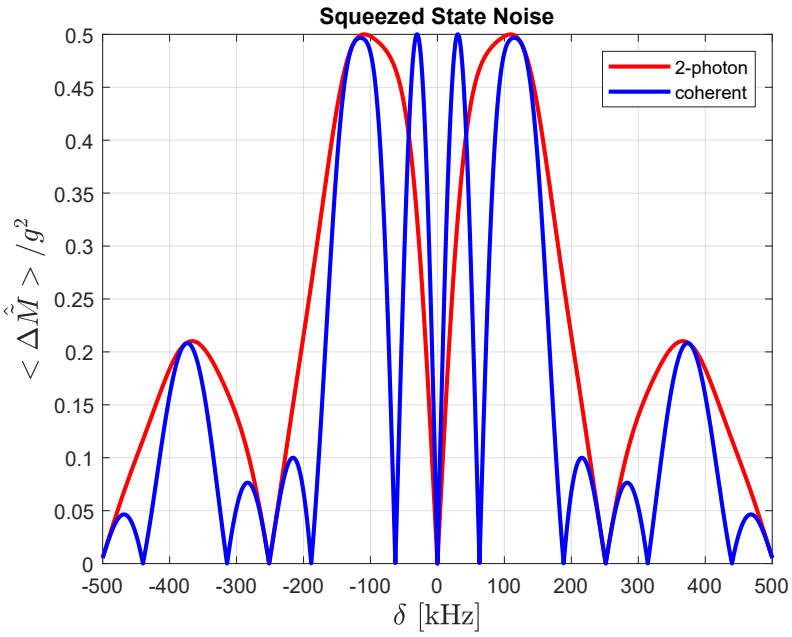

Figure 3.4. Two-photon squeezing noise: $r_1 = r_2 = 1$, $\theta_1 = \theta_2 = 0$

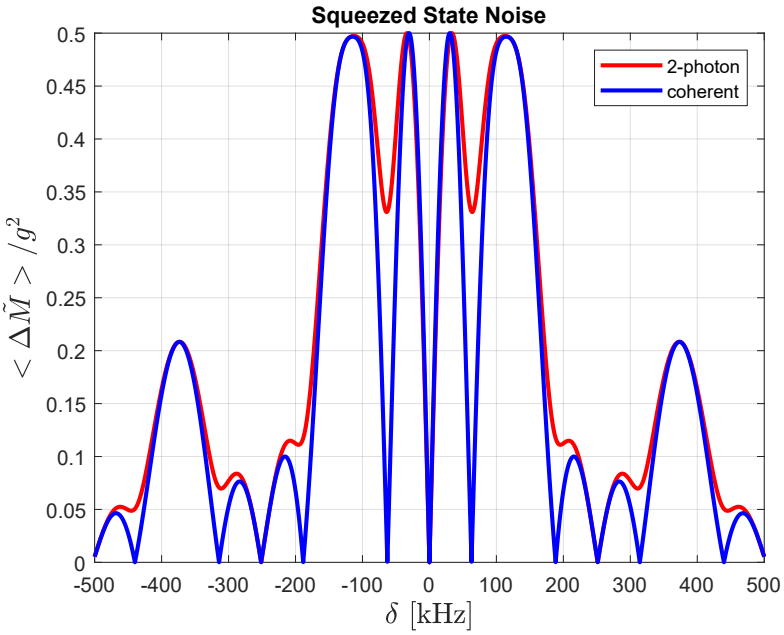

Figure 3.5. Two-photon squeezing noise: $r_1 = r_2 = 1$, $\theta_1 = \theta_2 = \pi/2$

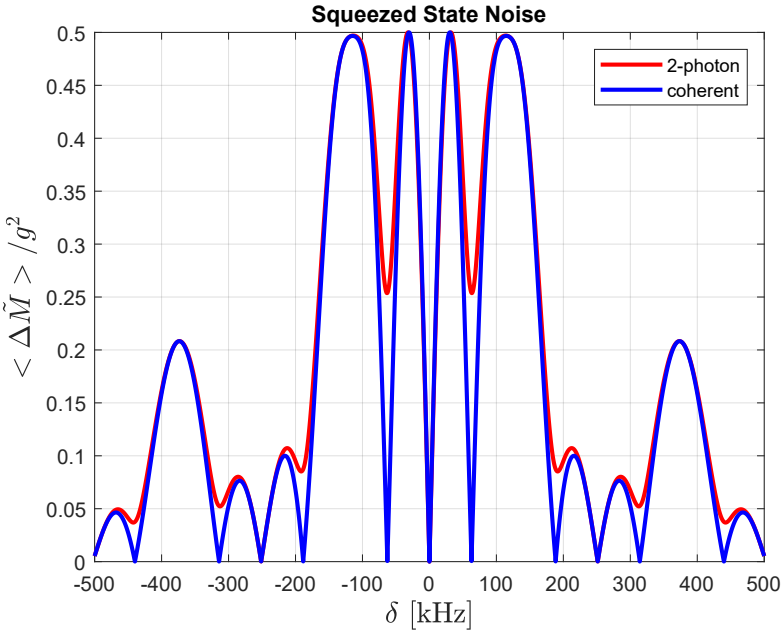

Figure 3.6. Two-photon squeezing noise: $r_1 = r_2 = 1$, $\theta_1 = \theta_2 = \pi$

THIS PAGE INTENTIONALLY LEFT BLANK

CHAPTER 4:
Experiments

4.1 Electromagnetically Induced Transparency

The initial setup for this experiment began with conducting experiments to achieve electromagnetically induced transparency (EIT). EIT is an interference phenomenon that occurs when a three-level atom is driven by a coherent field that makes a non-linear medium transparent to the probing field [18]. Our probe and pump fields are on single photon resonance combined in a medium, which in our case is ^{85}Rb. When combined in the medium as described, the pump laser splits the bare state energy level into two levels called dressed states [35]. The dressed states have energies $E + \frac{1}{2}\hbar\Omega$ and $E - \frac{1}{2}\hbar\Omega$, where Ω is the Rabi frequency of the pump laser as it drives its respective transition. This Rabi frequency is the same as in Equation 2.1b. When the pump laser is strong, the absorption spectrum of a weak probe laser shows two distinct peaks (two distinct resonances) separated in frequency by the Rabi frequency. This phenomenon is called Autler-Townes splitting [36], and can be seen in the blue trace in Figure 4.1. When the pump laser is also weak, then the probability amplitude of absorption between the two transitions destructively interferes and the absorption of the probe goes to zero. This phenomenon is known as EIT [37], which can be seen in the red trace of Figure 4.1.

The process used for squeezed light generation is four-wave mixing (FWM), which we talk about more in Section 4.3. Both EIT and FWM are based on generating coherence in an atomic medium (i.e., the same conditions are needed for EIT to work as FWM to work). However, there are fewer parameters in an EIT experiment to optimize, relative to the FWM experiment. Therefore, a logical first step in the FWM experiment is to observe EIT.

4.2 Experiment

EIT is not new and has been studied by [18], [35], [37]. As we mentioned in Section 4.1, much of the setup for EIT is similar to the setup for FWM to occur. By observing EIT we can confirm that our frequencies, ν_p and ν_{pr}, are set correctly. EIT and FWM also depends on whether all the laser fields are mutually coherent. Since all the laser fields used

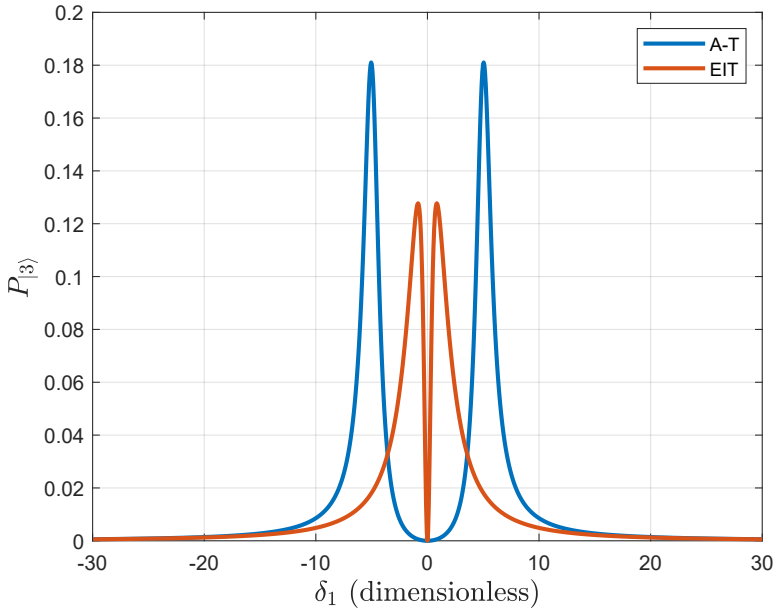

Figure 4.1. Plot of excited state probability showing Autler-Townes ($\Omega_2 = 10$) splitting and EIT ($\Omega_2 = 1$). Other parameters: $\Omega_1 = 1, \delta_2 = 0$.

are derived from a single laser source we have the logical expectation that we can observe EIT and FWM. We began with a 780nm distributed feedback laser (DFB) tuned to the $F = 2 \rightarrow F'$ transition of ^{85}Rb, which is the weaker of the two hyperfine transitions. Of note, we omit the upper state quantum number F because the states are unresolved within a Doppler medium. The light then passes through a series of optics to a high frequency acousto-optic modulator (HFAOM), as seen in Figure 4.2.

To achieve the desired 3 GHz frequency shift between the probe and pump beam, the laser goes through the HFAOM. The first order from the first pass through the HFAOM shifts the frequency of the laser up approximately 1.5GHz. The first order up-shifted beam from the first pass is coupled into a fiber and becomes our pump beam, ν_p. The retroflected beam passes through the HFAOM and is downshifted 1.5GHz. This beam eventually becomes our probe beam, ν_{pr}.

To achieve independent frequency control between the pump and probe beam, the down-shifted beam is sent through a low frequency acousto-optic modulator (LFAOM). As mentioned before, the interference between two possible absorption pathways to get to the

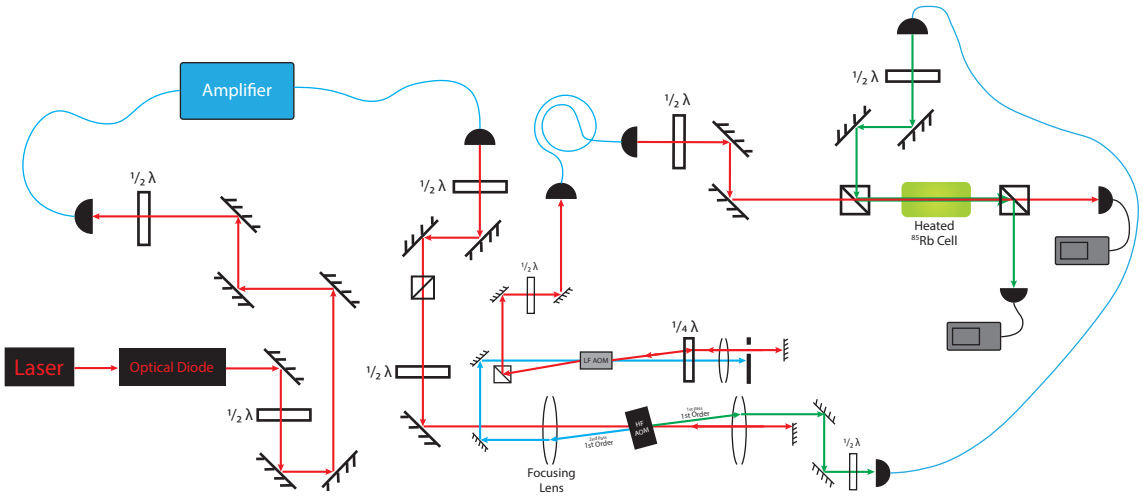

Figure 4.2. EIT experiment schematic.

E_3 energy level causes EIT. By setting up the experiment to scan the probe, we are scanning between those two dressed states. This is necessary for our EIT experiment to work. We can scan the probe frequency independent of the pump frequency even though they originate from the same laser by scanning the radio frequency that drives the LFAOM. In order to prevent the fiber couple efficiencies and power fluctuations that go along with scanning in this manner, we did another dual pass of the down shifted beam through the LFAOM. The resulting beam from the dual pass in the LFAOM is the probe beam, ν_{pr}.

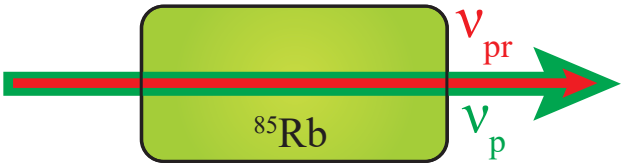

Figure 4.3. Laser alignment through Rb cell for the EIT experiment.

For EIT to occur, the pump and probe beam were set up to overlap each other using a polarizing beam splitter, which is how the EIT experiment varies from FWM experiment. The two spatially overlapping beams were then sent through a cell of isotopically pure ^{85}Rb as depicted in Figure 4.3. EIT occurs when frequencies of the pump and the probe are set to

Δ apart from each other. In this respect, the FWM and EIT experiments are alike and it is for this reason that the EIT experiment is important. To determine the exact frequencies needed to set ν_p and ν_{pr} a frequency Δ apart from each other in their respective configurations, we calculated

$$\begin{aligned} \Delta &= \nu_p - \nu_{pr} \\ \Delta &= \left(\nu_L + \nu_{hf}\right) - \left(\nu_L - \nu_{hf} + 2\nu lf\right) \\ \Delta &= 2\left(\nu_{hf} - \nu_{lf}\right) \\ \nu_{hf} &= \frac{\Delta}{2} + \nu_{lf}, \end{aligned} \tag{4.1}$$

where ν_L is the frequency of the laser, ν_{hf} is the HFAOM frequency shift, ν_{lf} is the LFAOM frequency shift which is equal to 73.6 MHz, a value that is approximately the frequency for optimal LFAOM efficiency, and Δ as stated before is the hyperfine splitting frequency for ^{85}Rb, which equals 3035.7 MHz [33]. This derivation is used for an up-shifted pump beam and a downshifted probe beam, but those can be switched by starting with $\Delta = \nu_{pr} - \nu_p$ and slight setup changes. From Equation 4.1 we determined for our experiment $\nu_{hf} = 1444.25$ MHz. We set up the LFAOM with a linear scan of ±6.0 MHz.

EIT Data

As we scan the LFAOM, there was a peak in the transmission of both the pump and the probe. Figure 4.4 shows the pump transmission for several values of the probe power, while Figure 4.5 shows the probe transmission for several values of the pump power. Looking at the pump transmission (Figure 4.4), we see that the transmission decreases as the probe power increases, but the spike in transmission at around two-photon detuning becomes increasingly apparent. Experimentally, this supports that EIT was occurring, which is explained by the three-level atom diagram, Figure 2.3. When the probe laser is on and very weak, there will be very few atoms that will be optically pumped into state $|2\rangle$. When the probe beam is on and strong, there will be more atoms optically pumped into state $|2\rangle$. The more atoms that are available in state two, the more atoms are available to absorb the pump (i.e., decreased transmission). As the probe beam increases in power from .05mW to .65mW there was a constant decrease in transmission of the pump beam, but a sharper and sharper transmission curve around two-photon resonance. The data here also supports

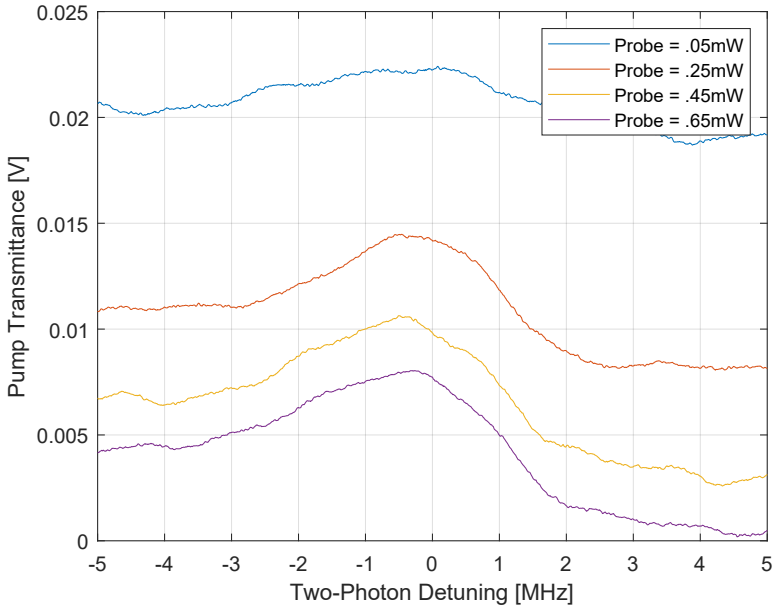

Figure 4.4. Pump transmission vs two-photon detuning for varying probe powers.

that EIT was in fact occurring, and was the cause for the spike in transmission around two-photon detuning.

The line shape of this data also leads us to believe that this was in fact EIT. One could argue that the line shape we have now is not easily fit to a Lorenztian distribution, which in theory is what an EIT signal should look like [37]. On that basis, one might argue that this data in fact does *not* represent EIT. However, the asymmetry in the plot was caused by changes in LFAOM efficiencies as we scanned. If the peak of the efficiency scan does not coincide with the peak of the two-photon resonance, then there will be an asymmetry in the readings, which is what the data shows here.

The full width at half maximum (FWHM) of the peaks were measured. Specifically, the FWHM of the data taken when the probe power was .25mW was examined. A measurement of the linewidth for a probe power of 0.05mW would have been better but the signal to noise ratio was too small. The result was approximately 2.5MHz which is less than the full natural linewidth in ^{85}Rb of 6MHz [33]. EIT is a sub-natural linewidth phenomenon [35]. The measurement of the linewidth being sub-natural linewidth is further evidence this was in

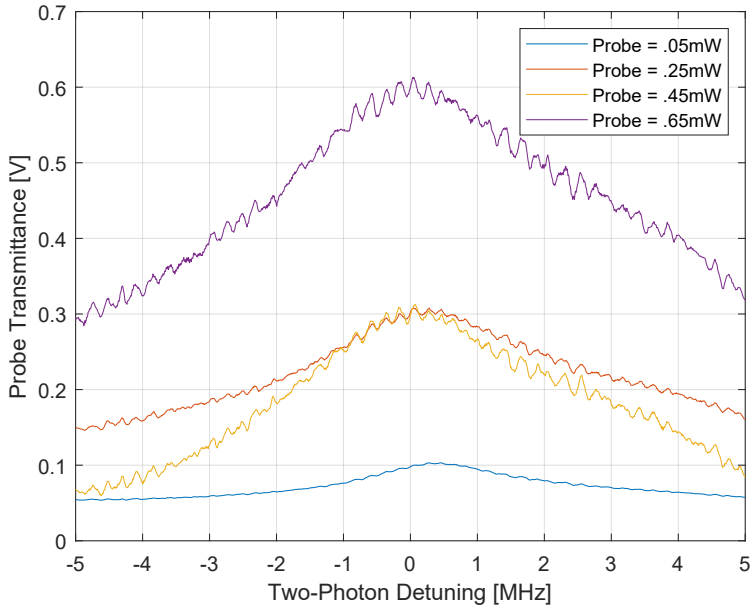

Figure 4.5. Probe transmission vs two-photon detuning for varying probe powers.

fact EIT.

The correlating data from the probe beam also confirms EIT was occurring. Here, we are looking for an increase in transmission as the probe power increases, which was exactly what was found. Along with the transmission increasing, we also saw the transmission spike at around two-photon detuning which became narrower as the power increased, with the most obvious peak occurring when the probe was set to .65mW.

These series of experiments demonstrate the system has the required conditions of coherence, laser power and laser frequencies for FWM to occur. The next step is to demonstrate FWM, which requires a few changes to the experiment.

4.3 Four-Wave Mixing

FWM is the name given for the process that produces the squeezed light described in Section 3.2. This section discusses the physics for efficient FWM to occur, as well as explain the details regarding how to setup a FWM experiment. Also described are our attempts at

producing squeezed light by modifying the EIT set up from Section 4.2. Like EIT, FWM is not a new process and has been successfully demonstrated by many teams [38], [39]. Below, we discuss a FWM setup used and explained by [38].

FWM occurs when an orthogonally polarized pump and probe beam, ν_p and ν_{pr}, respectively, are crossed inside of a non-linear medium at a very small angle separated in frequency by the medium's ground state hyper-fine splitting frequency, Δ, and is depicted in Figure 4.6. This results in the production of a third conjugate beam [40] by way of the non-linear process described below. The conjugate beam holds the squeezing properties desired for the experiment and is quantum correlated to the probe beam. Since the two beams are quantum correlated, the measurements from the two beams are also correlated and can be used to reduce the amount of signal noise in the squeezed conjugate beam. The conjugate beam can then be used as Ramsey spectroscopy detector beams, and in other atomic interferometer applications to improve the accuracy and sensitivity of measurements [40].

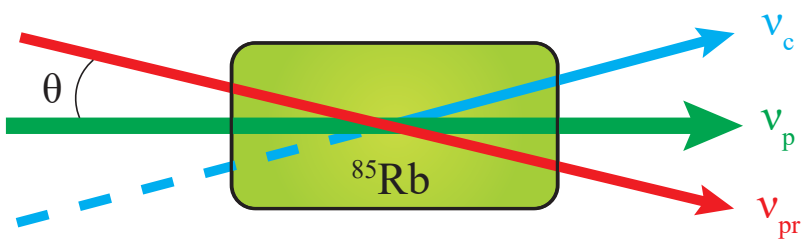

Figure 4.6. Laser alignment through Rb cell for the FWM experiment. Adapted from [38].

Figure 4.7 shows the atomic transitions that occur as the two beams cross inside the ^{85}Rb cell during the FWM process. As the two beams cross at a small angle inside the cell the pump beam excites a photon from the Rb which causes stimulated emission into the probe mode to occur. This photon emits with the probe beam and causes the atom to transition down the $F = 2$ energy state. It is for this reason that the probe experiences gain (i.e., the probe beam strength increases during the FWM process) [38]. While this occurs the ^{85}Rb atom absorbs another pump photon causing stimulated emission again but this time in the form of a conjugate beam at an angle opposite (with respect to the pump beam direction) and at the same polarization as the probe beam [40]. This emitted photon comprises the squeezed conjugate beam, ν_c. The FWM process can only occur if the frequency difference

between the pump and the probe beam is exactly ν_{hf}, where ν_{hf} is the ground state hyperfine splitting frequency between F_2 and F_3 states of ^{85}Rb.

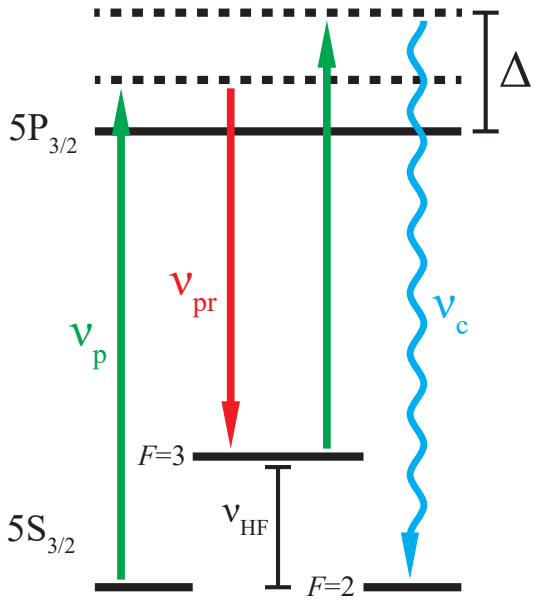

Figure 4.7. Atomic transitions used in the FWM process. Adapted from [38]

As stated before, the EIT and FWM setups are relatively the same with the changes shown in Figure 4.6. Another change to the setup is the addition of an amplifier to amplify ν_p so as to increase the gain experienced by the probe photons. The maximum power generated by the the amplifier was approximately 74mW, likely due to aging of the amplifier. Our entire FWM experiment schematic is seen in Figure 4.8.

This setup was determined after several iterations of failed attempts at producing squeezed light. The first attempt failed due to a lack of power from the HFAOM going into the amplifier to trigger a stable amplification of the pump beam. Due to the type of laser used for this experiment, and already being close to the limit of the power the laser could produce (65mW), this required the addition of an amplifier (also used in the EIT experiment). Once that amplifier was added, that problem was solved.

The next problem became the drastic difference between the powers of ν_p and ν_{pr}. Because of this difference it is difficult to distinguish between, or even determine if the conjugate

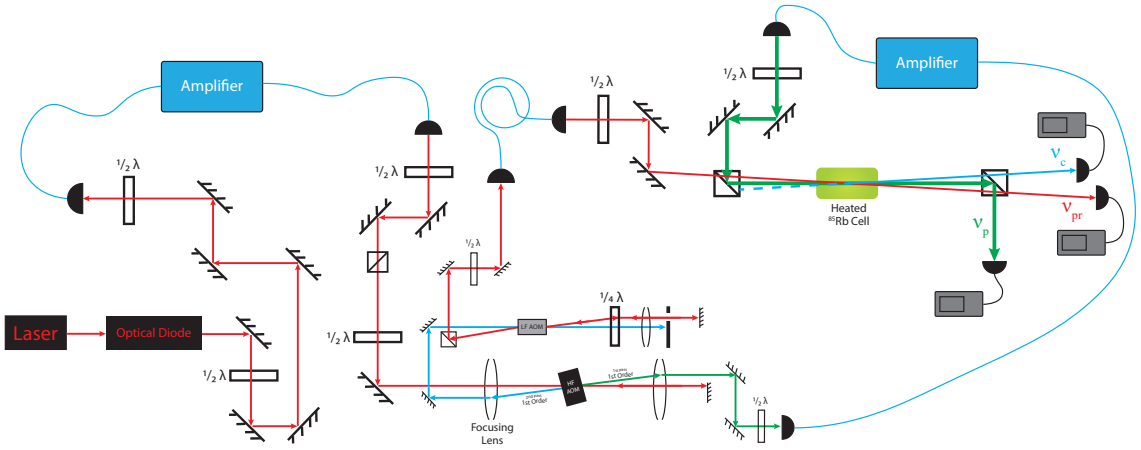

Figure 4.8. Laser alignment through Rb cell for the FWM experiment.

beam is being produced. This is due to the overwhelming radiance from the pump beam which washes out any evidence of a weak conjugate beam. Due to the small angle the two beam must cross, and the confined physical experiment area, we are not able to allow the beams to propagate far enough to separate the beams by enough space to distinguish the conjugate beam from the pump and probe beams. A beam blocker did not work either as the radiance was still too bright.

Taking into account these experimental issues, the final setup is shown in Figure 4.8. Previous work shows that the conjugate beam will have the same polarization as the probe beam [38]. Taking advantage of the orthogonal polarization of the pump versus the conjugate beam, a polarizing beam splitter was added after the ^{85}Rb cell to separate the two beams away from each other and directed towards photo-detectors. This separated the beams by 90° allowing a determination as to whether a conjugate beam was being produced.

Time constraints prevented the actual demonstration of FWM. However, the results of this chapter indicate that future students will be able to demonstrate FWM without major modifications to the experimental apparatus.

THIS PAGE INTENTIONALLY LEFT BLANK

CHAPTER 5:
Discussion and Conclusions

With heavy reliance on GPS and the ever-growing threat of cyber attacks, there is a need for improved INS with increased sensitivity and accuracy. This improvement is a must for the the Navy and Marine Corps to regain our dominance in the sea, air, and land. The integration of FWM and squeezed light with atom interferometers holds that potential, and this thesis has laid the groundwork for the development and testing in such a system.

The main achievement from this thesis was building the EIT setup and successfully observing the effects of EIT through hot ^{85}Rb vapor. With demonstrated experimental results and observations of EIT, further work can be done to tune the lasers to amplify the probe signal. By making the signal stronger and more distinguishable from the pump, the likelihood of producing FWM will increase. One method that can accomplish this improvement is to expand the pump laser's diameter before the pump laser enters the Rb cell and mixes with the probe laser. By increasing the diameter of the pump beam, we increase the amount of time that the atoms have to interact with each other and the Rb atoms, which increases the coherence of the medium. Once this is properly built, setup, and tuned, the next step is FWM.

The second achievement from this thesis was the eventual design of an experiment to observe FWM through some result of trial, error, and redesign. Initially, this experiment started with attempting to produce FWM before producing EIT. Later, we learned that perhaps a more logical order of events should be EIT then FWM. Through trial and error of producing a FWM experiment, an experimental design was developed that can produce and detect FWM, with all of this proven by our successful EIT experiment and the findings of this thesis. Although FWM was not observed during our attempts, the groundwork was laid, as discussed in Section 4.3, and a foundation set for further work on the EIT experiment, leading into FWM.

Lastly, the third achievement of this thesis was deriving the calculations for expected noise improvements between coherent and squeezed light. Theoretically, there is a significant chance for noise reduction in the detector beams once the FWM experiment becomes operational.

Upon completion of the FWM experiment, the resulting conjugate beam can be used in Ramsey spectroscopy measurements throughout the NPS Quantum Sensors Lab lab where an increase in accuracy and sensitivity of measurements will be seen. By accomplishing this, it would be a substantial step forward for drastically improving the capabilities for navigation in the Navy apart from GPS.

APPENDIX A:
MATLAB Code

Rabi Oscillations

```
close all

t = [0:0.1:4*pi];

% No Detuning
Omega_1 = 1; % [MHz]
delta_1 = 0; % [MHz]
Omegaprime_1 = sqrt(abs(Omega_1)^2 + delta_1^2);
P2_1 = .5*abs(Omega_1/Omegaprime_1)^2 * (1-cos(Omegaprime_1*t));

% Detuned delta_1
Omega_2 = 1.0; % [MHz]
delta_2 = .75; % [MHz]
Omegaprime_2 = sqrt(abs(Omega_2)^2 + delta_2^2);
P2_2 = .5*abs(Omega_2/Omegaprime_2)^2 * (1-cos(Omegaprime_2*t));

% Detuned delta_2
Omega_3 = 1; % [MHz]
delta_3 = 1.25; % [MHz]
Omegaprime_3 = sqrt(abs(Omega_3)^2 + delta_3^2);
P2_3 = .5*abs(Omega_3/Omegaprime_3)^2 * (1-cos(Omegaprime_3*t));

figure(1)
plot(t,P2_1,'LineWidth',2);
hold on
plot(t,P2_2,'LineWidth',2);
plot(t,P2_3,'k','LineWidth',2);
xt = get(gca, 'XTick');
set(gca, 'FontSize', 12)

grid on
xticks([0*pi pi 2*pi 3*pi 4*pi]);
xticklabels({'0\pi','\pi','2\pi','3\pi','4\pi'});
xlim([0 4*pi]);
xlabel('\Omega^{\prime}(t)','FontSize',14);
ylabel('P_{|2\rangle}','FontSize',14);
legend('\delta = 0 MHz','\delta = .75 MHz','\delta = 1.25
 MHz','Location','North');
```

Raman Plot

```
close all

Tpulse = 25e-6;
t = Tpulse; % [s]
OmegaR = pi/Tpulse;
delta2p = linspace(-1e6,1e6,2000); % [Hz]
OmegaRprime = sqrt(abs(OmegaR).^2 + delta2p.^2);

P2 = .5*abs(OmegaR./OmegaRprime).^2 .* (1-cos(OmegaRprime*t));

plot(delta2p./1000,P2,'LineWidth',2);
grid on

title('Raman Probability');
xlabel('\delta [kHz]','FontSize',14);
ylabel('P_{|2\rangle}','FontSize',14);
```

Plotting Measurement Operator and Noise - Coherent State

```
close all;

% Variables

g = 1; % coupling constant
delta = linspace(-5e5,5e5,1e4); % [Hz]
tau = 25e-6; % [s]
ftau = (exp(1i*delta*tau)-1) ./ (1i*delta);
alpha1 = 1.0;
alpha2 = 1.0;
theta = 0; % phase
T = 2.5e-5; % [s]

M = abs(g).^2.*abs(ftau).^2.*(abs(alpha1).^2 + abs(alpha2).^2 +...
    2.*alpha1.*alpha2.*cos(theta + delta.*(T+tau)));
Mtilde = M./max(M);

figure(1)
plot(delta./1000,Mtilde,'b','LineWidth',2);
grid on
title('Measurement Operator');
xlabel('\delta [kHz]','FontSize',14);
ylabel('$<\hat{M}>/g^2$','Interpreter','LaTeX','FontSize',14)

DeltaM = sqrt(M.*(1-M));
DeltaMTilde = sqrt(Mtilde.*(1-Mtilde));

figure(2)
plot(delta./1000,DeltaMTilde,'b','LineWidth',2);
grid on
title('Coherent State Noise');
xlabel('$\delta$ [kHz]','Interpreter','LaTeX','FontSize',14);
ylabel('$<\Delta \hat{\tilde{M}}>/
g^2$','Interpreter','LaTeX','FontSize',14)
```

Plotting Measurement Operator and Noise - Squeezed State

```
clear variables;
close all;
clc;

% Variables

alpha(1)=input('Enter alpha 1 ==> ');
alpha(2)=input('Enter alpha 2 ==> ');
r(1)=input('Enter squeezing parameter r1 ==> ');
theta(1)=input('Enter theta 1 ==> ');
r(2)=input('Enter squeezing parameter r2 ==> ');
theta(2)=input('Enter theta 2 ==> ');

g = 1; % coupling constant
delta = linspace(-5e5,5e5,1e4); % [Hz]
tau = 25e-6; % [s]
ftau = (exp(1i*delta*tau)-1) ./ (1i*delta);
phi = 0; % phase
T = 2.5e-5; % [s]

%   2-photon coherent state
mu=cosh(r);
nu=exp(1i*theta).*sinh(r);
alphatildemin=mu.*alpha-nu.*conj(alpha);
n(1)=alphatildemin(1).*conj(alphatildemin(1))+nu(1)*conj(nu(1));
n(2)=alphatildemin(2).*conj(alphatildemin(2))+nu(2)*conj(nu(2));

I1=alphatildemin(1).*conj(alphatildemin(1))+nu(1)*conj(nu(1))+...
    alphatildemin(2).*conj(alphatildemin(2))+nu(2)*conj(nu(2))+...
    alphatildemin(1)*conj(alphatildemin(2))*exp(1i*(phi + delta.*(T
+tau)))+...
    alphatildemin(2)*conj(alphatildemin(1))*exp(-1i*(phi + delta.*(T
+tau)));

M1 = abs(g).^2.*abs(ftau).^2.*(I1);
fid=figure('units','normalized','outerposition',[.05 .35 .35 .55]);

hold on
%
%  coherent state
%
r=[0 0];
mu=cosh(r);
nu=exp(1i*theta).*sinh(r);
alpha(1)=sqrt(n(1));
alpha(2)=sqrt(n(2));

I3=alpha(1).*conj(alpha(1))+nu(1)*conj(nu(1))+...
```

```
    alpha(2).*conj(alpha(2))+nu(2)*conj(nu(2))+...
    alpha(1)*conj(alpha(2))*exp(1i*(phi + delta.*(T+tau)))+...
    alpha(2)*conj(alpha(1))*exp(-1i*(phi + delta.*(T+tau)));
M3 = abs(g).^2.*abs(ftau).^2.*(I3);

figure(1)
plot(delta./1000,M1./max(M1),'r','LineWidth',2);
plot(delta./1000,M3./max(M3),'b','LineWidth',2);
legend('2-photon','coherent')
grid on
title('Squeezed Measurement Operator');
xlabel('$\delta$ [kHz]','Interpreter','LaTeX','FontSize',14);
ylabel('$<\hat{M}>/g^2$','Interpreter','LaTeX','FontSize',14)

% Delta M
% Coherent
Mtilde_C = M3/max(M3);
DeltaM_C = sqrt(M3.*(1-M3));
DeltaMtilde_C = sqrt(Mtilde_C.*(1-Mtilde_C)); %<-- this one

% Two-Photon
Mtilde_2 = M1/max(M1);
DeltaMtilde_2 = sqrt(Mtilde_2.*(1-Mtilde_2));

figure(2) %normalized DeltaM
plot(delta./1000,DeltaMtilde_2,'r','LineWidth',2);
grid on
hold on
plot(delta./1000,DeltaMtilde_C,'b','LineWidth',2); xlabel('$
\delta$ [kHz]','Interpreter','LaTeX','FontSize',14);
ylabel('$<\Delta \hat{\tilde{M}}>/
g^2$','Interpreter','LaTeX','FontSize',14)
title('Squeezed State Noise');
legend('2-photon','coherent');
```

Autler-Townes and EIT Plot

```
% This program plots the steady state single time averages for a
 driven
% three level atom with two laser fields in the lambda configuration.
%
% This program assumes monochromatic excitation of a closed system
 with
% no Doppler averaging in the radiative limit.
%
% The program keeps del-2 fixed and scans del-1

clear;

% For Autler Townes
% Enter W32 ==> 1
% Enter W21 ==> 0
% Enter omega-1 ==> 1
% Enter omega-2 ==> 10
% Enter delta-2 ==> 0
% Enter maximum frequency excusion for del-1 ==> 30

% For EIT
% Enter W32 ==> 1
% Enter W21 ==> 0
% Enter omega-1 ==> 1
% Enter omega-2 ==> 1
% Enter delta-2 ==> 0
% Enter maximum frequency excusion for del-1 ==> 30

% User inputs
%
disp('All rates scaled to W31');
W32=input('Enter W32 ==> ');
W21=input('Enter W21 ==> ');
om1=input('Enter omega-1 ==> ');
om2=input('Enter omega-2 ==> ');
del2=input('Enter delta-2 ==> ');
delmax=input('Enter maximum frequency excusion for del-1 ==> ');

%
% Minor Calculation section
%
ga12=0.5*W21;
ga13=0.5*(1+W32);
ga23=0.5*(1+W21+W32);
%
% Construct the matrix
%

npts=1000;
L=zeros(8,8);
```

```
Imat=zeros(8,1);
Res=zeros(8,1);
w=zeros(1,npts);
yplot=zeros(8,npts);

L(1,:)=[0 0.5*i*om2 0 0 0 0 -i*0.5*om1 0];
L(2,:)=[+0.5*i*om2 0 0 -0.5*i*om1 0 0 0 -i*om1];
L(3,:)=[0 0 0 0 +0.5*i*om1 -0.5*i*om2 0 0];
L(4,:)=[0 0 0 -W21 +0.5*i*om2 0 -0.5*i*om2 W32];
L(5,:)=[0 0 0.5*i*om1 0.5*i*om2 0 0 0 -0.5*i*om2];
L(6,:)=[0 0 -0.5*i*om2 0.5*i*om1 0 0 0 i*om1];
L(7,:)=[-0.5*i*om1 0 0 -0.5*i*om2 0 0 0 +0.5*i*om2];
L(8,:)=[0 -0.5*i*om1 0 0 -0.5*i*om2 0.5*i*om1 0.5*i*om2 -(1+W32)];
Imat=[0 0.5*i*om1 0 0 0 -0.5*i*om1 0 0].';
for n=1:npts
   w(n)=-delmax+2*n*delmax/npts;
   del1=w(n);
   L(1,1)=-(ga12-i*(del2-del1));
   L(2,2)=-(ga13+i*del1);
   L(3,3)=-(ga12+i*(del2-del1));
   L(5,5)=-(ga23+i*del2);
   L(6,6)=-(ga13-i*del1);
   L(7,7)=-(ga23-i*del2);

   Res=-inv(L)*Imat;
   yplot(:,n)=Res(:);
end
%
% Plot the results
iplot=1;
while (iplot>=1)&(iplot<=8)
 disp('To plot rho-12 ... enter 1');
 disp('To plot rho-13 ... enter 2');
 disp('To plot rho-21 ... enter 3');
 disp('To plot rho-22 ... enter 4');
 disp('To plot rho-23 ... enter 5');
 disp('To plot rho-31 ... enter 6');
 disp('To plot rho-32 ... enter 7');
 disp('To plot rho-33 ... enter 8');
   iplot=input(' ');
   if (iplot>8)|(iplot<1)
      break
   end

   %fid=figure;
   plot(w,real(yplot(iplot,:)),'LineWidth',2);
   grid on
   xlabel('$\delta_1$
 (dimensionless)','Interpreter','latex','FontSize',14)
   ylabel('$P_{|3 \rangle}$','Interpreter','latex','FontSize',14)
   pause;
   %close(fid);
end
```

EIT Data

```
close all;

load('EITData4_Workspace2.mat');
offset = 73.0;
freq = linspace(67.552,79.947,1563)'-offset;
xrange = 5.0; % [MHz]

% All data is vertical offset adjusted

% Pump Readings Varying Probe Power, Pump=1.0mW
figure(1)
plot(freq,smooth(Pr05_PmpConst{:,2}-.17));
hold on
plot(freq,smooth(Pr25_PmpConst{:,2}-.1588));
plot(freq,smooth(Pr45_PmpConst{:,2}-.1588));
plot(freq,smooth(Pr65_PmpConst{:,2}-.1496));

xlabel('Two-Photon Detuning [MHz]'); ylabel('Pump Transmittance [V]')
legend('Probe = .05mW','Probe = .25mW','Probe = .45mW','Probe
 = .65mW');
xlim([-xrange xrange]); % Scale for offset from two photon detuning
grid on;

% Probe Readings Varying Probe Power, Pump=1.0mW
figure(2)
plot(freq,smooth(Pr05_PmpConst{:,3}));
hold on
plot(freq,smooth(Pr25_PmpConst{:,3}-.222));
plot(freq,smooth(Pr45_PmpConst{:,3}-.656));
plot(freq,smooth(Pr65_PmpConst{:,3}-.796));
%plot(freq,smooth(Pr85_PmpConst{:,3}-.796));

xlabel('Two-Photon Detuning [MHz]'); ylabel('Probe Transmittance [V]')
legend('Probe = .05mW','Probe = .25mW','Probe = .45mW','Probe
= .65mW');
xlim([-xrange xrange]); % Scale for offset from two photon detuning
grid on;
```

List of References

[1] M. O. Scully and J. P. Dowling, "Quantum-noise limits to matter-wave interferometry," *Phys. Rev. A*, vol. 48, pp. 3186–3190, Oct 1993. Available: https://link.aps.org/doi/10.1103/PhysRevA.48.3186

[2] O. Carnal and J. Mlynek, "Young's double-slit experiment with atoms: A simple atom interferometer," *Physical Review Letters*, vol. 66, no. 21, pp. 2689–2692, May 1991, publisher: American Physical Society. Available: https://link.aps.org/doi/10.1103/PhysRevLett.66.2689

[3] F. Riehle, T. Kisters, A. Witte, J. Helmcke, and C. J. Bordé, "Optical Ramsey spectroscopy in a rotating frame: Sagnac effect in a matter-wave interferometer," *Physical Review Letters*, vol. 67, no. 2, pp. 177–180, July 1991, publisher: American Physical Society. Available: https://link.aps.org/doi/10.1103/PhysRevLett.67.177

[4] D. W. Keith, C. R. Ekstrom, Q. A. Turchette, and D. E. Pritchard, "An interferometer for atoms," *Physical Review Letters*, vol. 66, no. 21, pp. 2693–2696, May 1991, publisher: American Physical Society. Available: https://link.aps.org/doi/10.1103/PhysRevLett.66.2693

[5] M. Kasevich and S. Chu, "Atomic interferometry using stimulated Raman transitions," *Physical Review Letters*, vol. 67, no. 2, pp. 181–184, July 1991, publisher: American Physical Society. Available: https://link.aps.org/doi/10.1103/PhysRevLett.67.181

[6] M. Kasevich and S. Chu, "Measurement of the gravitational acceleration of an atom with a light-pulse atom interferometer," *Applied Physics B Photophysics and Laser Chemistry*, vol. 54, no. 5, pp. 321–332, May 1992. Available: http://link.springer.com/10.1007/BF00325375

[7] T. L. Gustavson, P. Bouyer, and M. A. Kasevich, "Precision Rotation Measurements with an Atom Interferometer Gyroscope," *Physical Review Letters*, vol. 78, no. 11, pp. 2046–2049, Mar. 1997. Available: https://link.aps.org/doi/10.1103/PhysRevLett.78.2046

[8] A. Lenef, T. D. Hammond, E. T. Smith, M. S. Chapman, R. A. Rubenstein, and D. E. Pritchard, "Rotation Sensing with an Atom Interferometer," *Physical Review Letters*, vol. 78, no. 5, pp. 760–763, Feb. 1997, publisher: American Physical Society. Available: https://link.aps.org/doi/10.1103/PhysRevLett.78.760

[9] A. Peters, K. Y. Chung, and S. Chu, "High-precision gravity measurements using atom interferometry," *Metrologia*, vol. 38, no. 1, pp. 25–61, Feb.

2001. Available: http://stacks.iop.org/0026-1394/38/i=1/a=4?key=crossref.33bae2a3cd81df1aadcc7dc5746aa663

[10] P. R. Berman, *Atom Interferometry*. Academic Press, Jan. 1997.

[11] J. Baudon, R. Mathevet, and J. Robert, "Atomic interferometry," *Journal of Physics B-Atomic Molecular and Optical Physics*, vol. 32, no. 15, pp. R173–R195, Aug. 1999.

[12] A. D. Cronin, J. Schmiedmayer, and D. E. Pritchard, "Optics and interferometry with atoms and molecules," *Reviews of Modern Physics*, vol. 81, no. 3, pp. 1051–1129, Sep. 2009.

[13] R. Geiger, A. Landragin, S. Merlet, and F. Pereira Dos Santos, "High-accuracy inertial measurements with cold-atom sensors," *AVS Quantum Science*, vol. 2, no. 2, p. 024702, June 2020, publisher: American Vacuum Society. Available: https://avs.scitation.org/doi/10.1116/5.0009093

[14] B. Barrett, A. Bertoldi, and P. Bouyer, "Inertial quantum sensors using light and matter," *Physica Scripta*, vol. 91, no. 5, p. 053006, Apr. 2016, publisher: IOP Publishing. Available: https://doi.org/10.1088%2F0031-8949%2F91%2F5%2F053006

[15] K. Bongs, M. Holynski, J. Vovrosh, P. Bouyer, G. Condon, E. Rasel, C. Schubert, W. P. Schleich, and A. Roura, "Taking atom interferometric quantum sensors from the laboratory to real-world applications," *Nature Reviews Physics*, vol. 1, no. 12, pp. 731–739, Dec. 2019. Available: http://www.nature.com/articles/s42254-019-0117-4

[16] N. P. Robins, P. A. Altin, J. E. Debs, and J. D. Close, "Atom lasers: Production, properties and prospects for precision inertial measurement," *Physics Reports*, vol. 529, no. 3, pp. 265–296, Aug. 2013. Available: http://www.sciencedirect.com/science/article/pii/S037015731300118X

[17] F. A. Narducci, A. T. Black, and J. H. Burke, "Advances toward fieldable atom interferometers," *Advances in Physics: X*, vol. 7, no. 1, p. 1946426, 2022. Available: https://doi.org/10.1080/23746149.2021.1946426

[18] M. Scully and M. Zubairy, *Quantum Optics* (Quantum Optics). Cambridge University Press, 1997. Available: https://books.google.com/books?id=20ISsQCKKmQC

[19] L. Mandel and E. Wolf, *Optical Coherence and Quantum Optics*. Cambridge University Press, 1995, p. 741–804.

[20] C. Gerry and P. Knight, *Introductory Quantum Optics*. Cambridge University Press, 2004, p. 74–114.

[21] R. Shankar, *Principles of Quantum Mechanics*. New York, NY: Plenum, 1980, pp. 353–371. Available: https://cds.cern.ch/record/102017

[22] C. Cohen-Tannoudji, B. Diu, and F. Laloë, *Quantum mechanics; 1st ed.* New York, NY: Wiley, 1977, pp. 773–803, trans. of : Mécanique quantique. Paris : Hermann, 1973. Available: https://cds.cern.ch/record/101367

[23] L. deBroglie, "Recherches sur la théorie des quanta (researches on the quantum theory)," *Ann. de Physique*, vol. 10, no. 3, p. 22, 1925.

[24] C. Foot and D. Foot, *Atomic Physics* (Oxford Master Series in Physics). OUP Oxford, 2005. Available: https://books.google.com/books?id=_CoSDAAAQBAJ

[25] M. M. Boyd, "High Precision Spectroscopy of Strontium in an Optical Lattice: Towards a New Standard for Frequency and Time," Ph.D. dissertation, University of Colorado, 2007.

[26] N. F. Ramsey, "A New Molecular Beam Resonance Method," *Physical Review*, vol. 76, no. 7, pp. 996–996, Oct. 1949, publisher: American Physical Society. Available: https://link.aps.org/doi/10.1103/PhysRev.76.996

[27] N. F. Ramsey, "A Molecular Beam Resonance Method with Separated Oscillating Fields," *Physical Review*, vol. 78, no. 6, pp. 695–699, June 1950, publisher: American Physical Society. Available: https://link.aps.org/doi/10.1103/PhysRev.78.695

[28] N. F. Ramsey, *Molecular Beams*. Oxford : Oxford ; New York: Oxford University Press, Apr. 1990.

[29] "The Nobel Prize in Physics 1989." Available: https://www.nobelprize.org/prizes/physics/1989/summary/

[30] N. F. Ramsey, "Experiments with separated oscillatory fields and hydrogen masers," *Reviews of Modern Physics*, vol. 62, no. 3, pp. 541–552, July 1990, publisher: American Physical Society. Available: https://link.aps.org/doi/10.1103/RevModPhys.62.541

[31] M. A. Lombardi, T. P. Heavner, and S. R. Jefferts, "NIST Primary Frequency Standards and the Realization of the SI Second," *NCSLI Measure*, vol. 2, no. 4, pp. 74–89, Dec. 2007. Available: https://ncsli.org/mpage/MJ_V2_A34

[32] H. J. Kimble and L. Mandel, "Theory of resonance fluorescence," *Phys. Rev. A*, vol. 13, pp. 2123–2144, Jun 1976. Available: https://link.aps.org/doi/10.1103/PhysRevA.13.2123

[33] D. Steck, "Rubidium 85 d line data," Sept. 2013, unpublished. Available: http://steck.us/alkalidata

[34] B. G. Levi, "Squeezing the quantum noise limits," *Physics Today*, vol. 39, no. 3, pp. 17–19, 1986. Available: https://doi.org/10.1063/1.2814922

[35] M. Fleischhauer, A. Imamoglu, and J. P. Marangos, "Electromagnetically induced transparency: Optics in coherent media," *Rev. Mod. Phys.*, vol. 77, pp. 633–673, Jul 2005. Available: https://link.aps.org/doi/10.1103/RevModPhys.77.633

[36] S. H. Autler and C. H. Townes, "Stark effect in rapidly varying fields," *Phys. Rev.*, vol. 100, pp. 703–722, Oct 1955. Available: https://link.aps.org/doi/10.1103/PhysRev.100.703

[37] S. E. Harris, J. E. Field, and A. Imamoğlu, "Nonlinear optical processes using electromagnetically induced transparency," *Phys. Rev. Lett.*, vol. 64, pp. 1107–1110, Mar 1990. Available: https://link.aps.org/doi/10.1103/PhysRevLett.64.1107

[38] N. Corzo, A. M. Marino, K. M. Jones, and P. D. Lett, "Multi-spatial-mode single-beam quadrature squeezed states of light from four-wave mixing in hot rubidium vapor," *Opt. Express*, vol. 19, no. 22, pp. 21 358–21 369, Oct 2011. Available: http://opg.optica.org/oe/abstract.cfm?URI=oe-19-22-21358

[39] A. I. Lvovsky, *Squeezed Light*. John Wiley & Sons, Ltd, 2015, ch. 5, pp. 121–163. Available: https://onlinelibrary.wiley.com/doi/abs/10.1002/9781119009719.ch5

[40] C. F. McCormick, A. M. Marino, V. Boyer, and P. D. Lett, "Strong low-frequency quantum correlations from a four-wave-mixing amplifier," *Phys. Rev. A*, vol. 78, p. 043816, Oct 2008. Available: https://link.aps.org/doi/10.1103/PhysRevA.78.043816

Initial Distribution List

1. Defense Technical Information Center
   Ft. Belvoir, Virginia

2. Dudley Knox Library
   Naval Postgraduate School
   Monterey, California